PhD candidate

FRANCESCO GIACOSA

Institute of Physics • Jan Kochanowski University
ul. Uniwersytecka 7 • 25-406 Kielce • Poland
nr album: 123456
First supervisor/promotor: prof. dr hab. h.c. mult. Amand Faessler
Second supervisor/ 2. promotor: prof dr hab. Thomas Gutsche
(add here auxiliary promotor(s), if existent)

fgiacosa@ujk.edu.pl
http://www.ujk.edu.pl/strony/Francesco.Giacosa/

PhD mid-term

1. Mid-term report / sprawozdanie śródokresowe
2. Presentation of mid-term achievements / Prezentacja
3. Publication list /wykaz publikacji
4. List of participation and talks/posters at scientific conferences / udział i wystąpienia lub postery na konferencjach naukowych
5. Talks at Institutes/Universities / wystąpienia na uniwersytetach/instytutach
6. Scientific internships /staży naukowe
7. Co-organization of conferences /Współorganizacja konferencji
8. Grants (internal and external, participation, accepted and/or sent) /granty
9. Query /kwerendy
10. Other activities (additional courses,) /inne
11. Print-out of publications

Place, date

Signature /podpis

Załącznik nr 5 do Regulaminu Szkoły Doktorskiej

SPRAWOZDANIE ŚRÓDOKRESOWE Z REALIZACJI INDYWIDUALNEGO PLANU BADAWCZEGO[1]

CZĘŚĆ I. INFORMACJE OGÓLNE:

Imię i nazwisko doktoranta:	
Numer albumu:	
Dziedzina/ dyscyplina naukowa lub artystyczna:	
Imię i nazwisko promotora lub promotorów:	
Imię i nazwisko promotora pomocniczego[2]:	

CZĘŚĆ II. ETAPY PRZYGOTOWANIA ROZPRAWY DOKTORSKIEJ LUB ARTYSTYCZNEJ:

Tematyka i plan pracy doktorskiej		
Temat rozprawy doktorskiej:		
Opis problematyki badawczej:		
Metody badawcze:		
Wstępna bibliografia:		
Rok kształcenia	**Etapy przygotowania rozprawy**	**Okres realizacji**

[1] Sprawozdanie wraz z załącznikami należy dostarczyć w formie papierowej (zbindowany dokument) oraz elektronicznej (na nośniku zewnętrznym, w jednym pliku PDF)

[2] w przypadku powołania promotora pomocniczego

CZĘŚĆ III. ZREALIZOWANE ZADANIA BADAWCZE W RAMACH INDYWIDUALNEGO PLANU BADAWCZEGO:

Rok kształcenia	Nazwa zadania badawczego lub artystycznego	Okres realizacji zadania	Efekt realizacji zadania[3]

CZĘŚĆ IV. EFEKTY DZIAŁALNOŚCI BADAWCZEJ – AKTYWNOŚCI PODNOSZĄCE KOMPETENCJE PRZYGOTOWUJĄCE DOKTORANTA DO PRACY O CHARAKTERZE BADAWCZYM LUB BADAWCZO-ROZWOJOWYM

Rok kształcenia	Aktywność	Okres realizacji

CZĘŚĆ V. DODATKOWE INFORMACJE, DOTYCZĄCE REALIZACJI INDYWIDUALNEGO PLANU BADAWCZEGO:

……

……

……

……

[3] Do sprawozdania należy dołączyć, w formie papierowej i elektronicznej, na nośniku zewnętrznym (w układzie zaproponowanym poniżej):
- wykaz publikacji z pełnymi zapisami bibliograficznymi, z podaniem nr ISBN, ISSN, DOI (udokumentowany w postaci kserokopii/skanów w formie elektronicznej artykułów naukowych, monografii, rozdziałów w monografii lub potwierdzeń z wydawnictwa o przyjęciu publikacji)
- wykaz konferencji, sesji posterowych (udokumentowany w postaci informacji o konferencji ze strony internetowej, potwierdzenie aktywnego udziału),
- potwierdzenie realizacji stażu,
- potwierdzenie udziału w organizacji konferencji naukowej,
- potwierdzenie złożenia wniosku o finansowanie badań do instytucji zewnętrznej lub numer umowy na realizację grantu lub portfolio zawierającego upublicznienia działań artystycznych,
- potwierdzenie otrzymania środków na badania z Uczelni,
- potwierdzenie udziału w projektach naukowych,
- opis kwerend,
- kserokopie dokumentów potwierdzających uzyskanie kompetencji np. certyfikat, udział w szkoleniu/kursie,
- wykaz innych aktywności
- prezentację multimedialną, zawierającą plan rozprawy doktorskiej, omówienie problematyki badawczej, metod badawczych.

……

……

……

……

……
(data i czytelny podpis doktoranta)

……
(data i czytelny podpis promotora/promotorów)

Układ dokumentów:

1. Strona tytułowa z danymi doktoranta
2. Sprawozdanie śródokresowe
3. Wydruk prezentacji multimedialnej
4. Wykaz publikacji
5. Wykaz aktywności naukowych:
   - konferencje,
   - sesje posterowe,
   - staże,
   - organizacja konferencji,
   - projekty badawcze (wnioski o finansowanie badań do instytucji zewnętrznej lub portfolio zawierające upublicznienia działań artystycznych: środki na badania z Uczelni),
   - kwerendy,
   - kursy, szkolenia,
   - inne.
6. Potwierdzenia działalności organizacyjnej na rzecz środowiska akademickiego i popularyzacji nauki

2. Presentation of mid-term achievements

Put the pdf of your presentation
(I put one as place-holder, which however is quite interesting 😊 – try to read it)

Mid-term presentation, Developments in Quantum Mechanics

Francesco Giacosa
UJK Kielce

Put here the talk to be presented at the mid-term exam

UJK Kielce, Poland
October 2021

(the talk has to be on your achievements in comparison to the plan presented in September 2020 as well as the plan for future)
Here I put something that you may find interesting as a place-holder
Remind: you have 10 minutes, so keep it short!)

Outline

1. Introduction
2. QM and philosophy (cats and many worlds)
3. QM, tunneling
4. Quantum computing
5. Final considerations

Quantum Mechanics

- One of the greatest achievements of human kind
- It describes small objects (atoms, particles,…)
- It is at the basis of physics and chemistry, as well as many applications
- A particle can be in two (or more) places at the same time

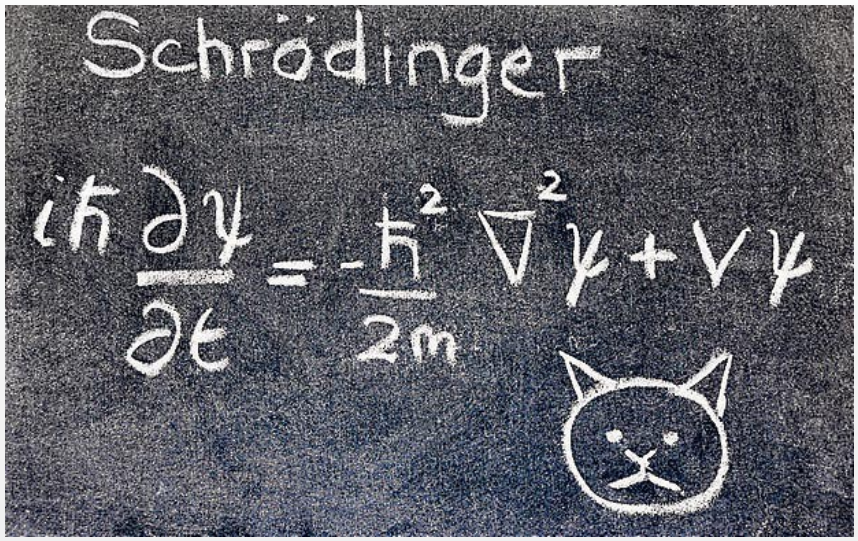

This equation describes a probability wave: it tells us where the particle „probably” is, but now where it is exactly.

Quantum Mechanics

E. Schroedinger 1887 - 1961

W. Heisenberg 1901-1976

QM uses all the mathematical properties described above:
Imaginary numbers, irrational numbers,
countable and uncountable infinities…

QM requires a lot of maths

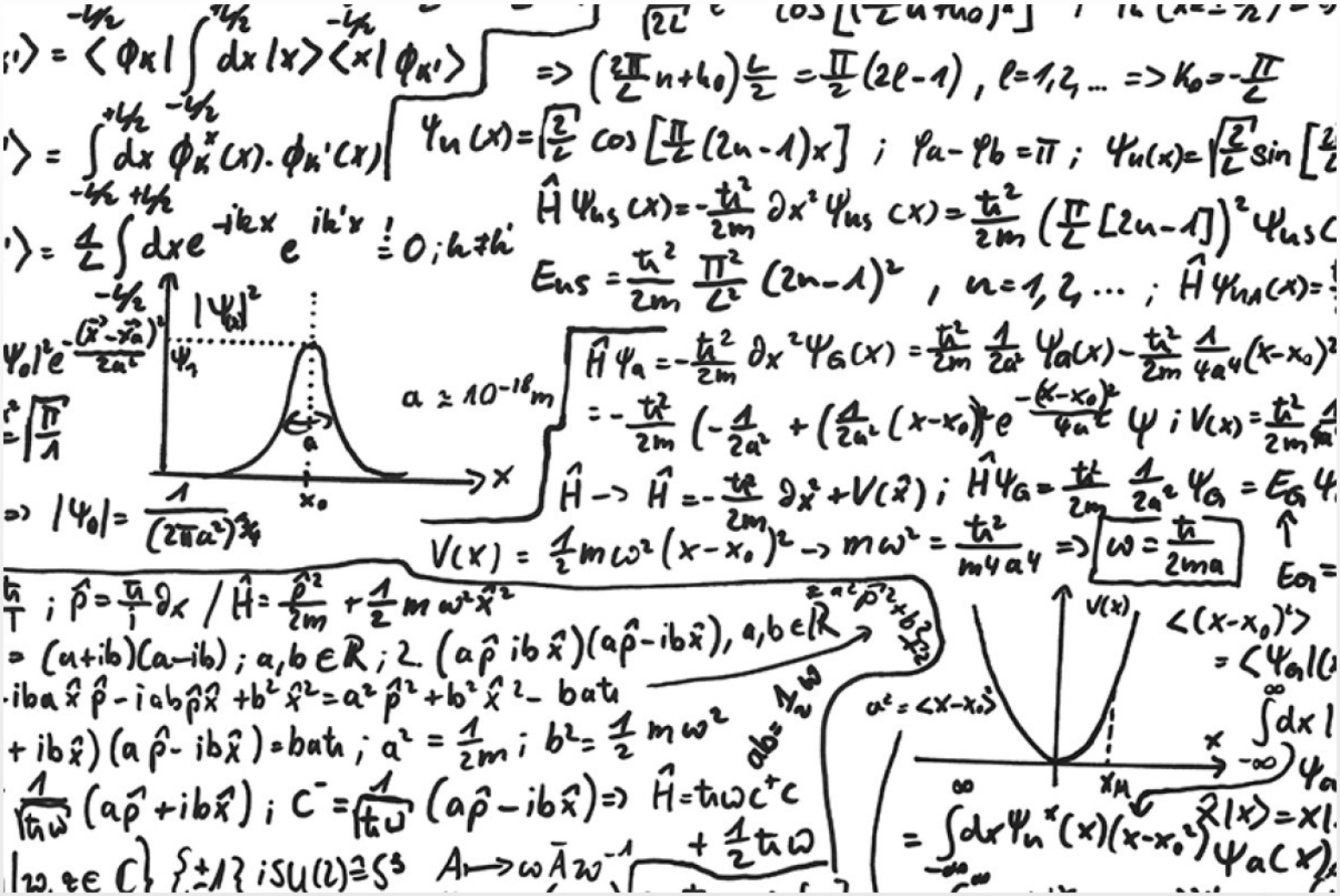

Interference, two-slit experiment

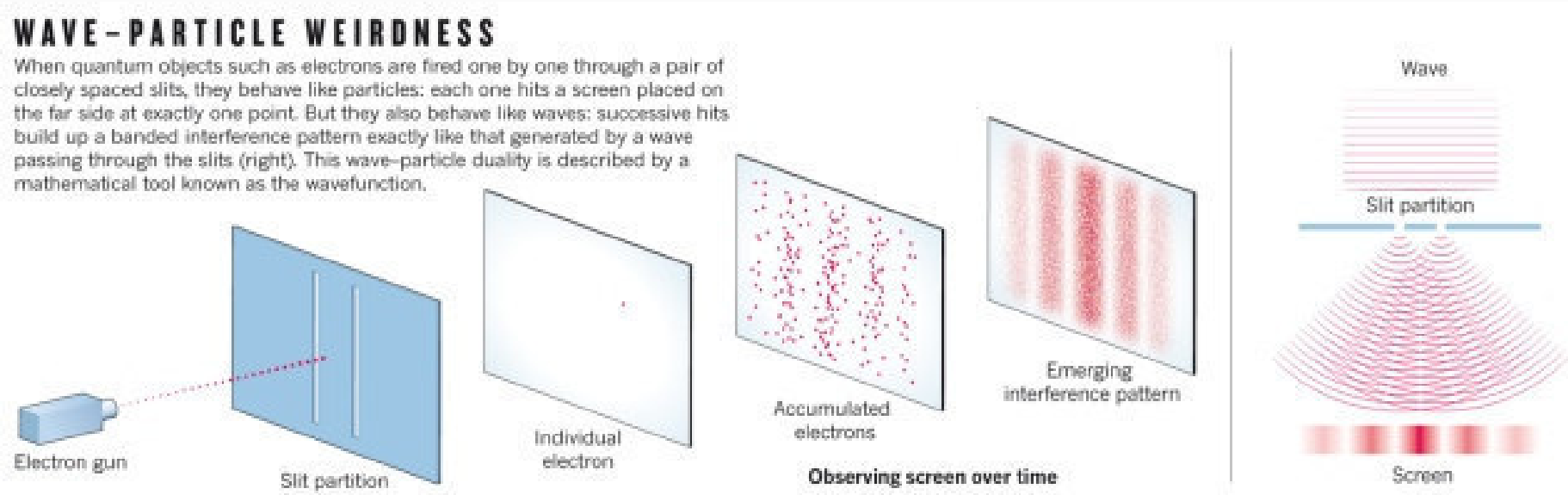

R. Feynman:
the **two-slit** experiment contains the "**one mystery**" of quantum mechanics.

The electron goes through both slits as a wave but then appear as a single spot (collapse) - on the screen.

Bohr vs. Einstein

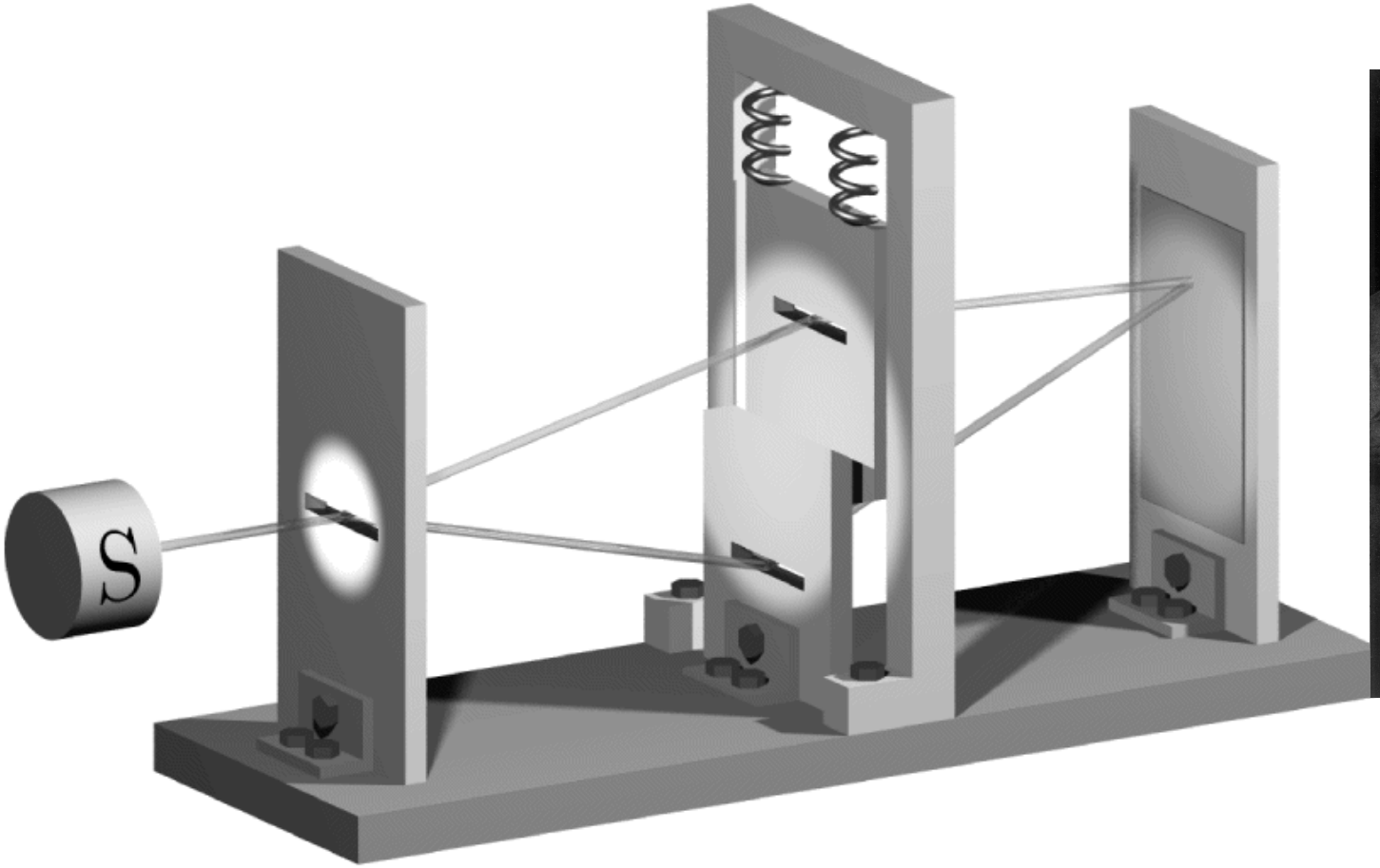

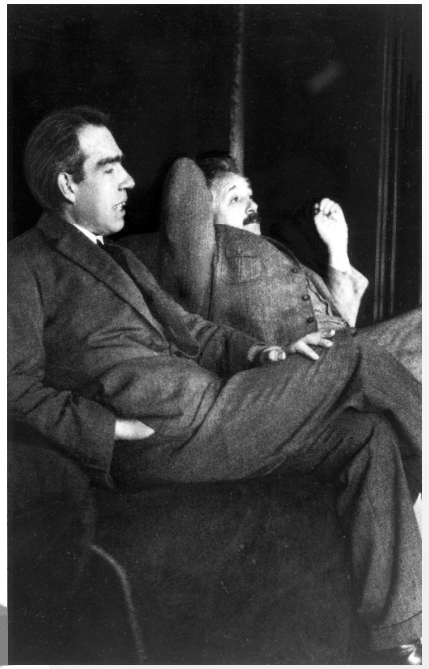

Einstein and Bohr debated long on the nautre of Quantum Theory.

Interference seen also for these ‘big’ objects

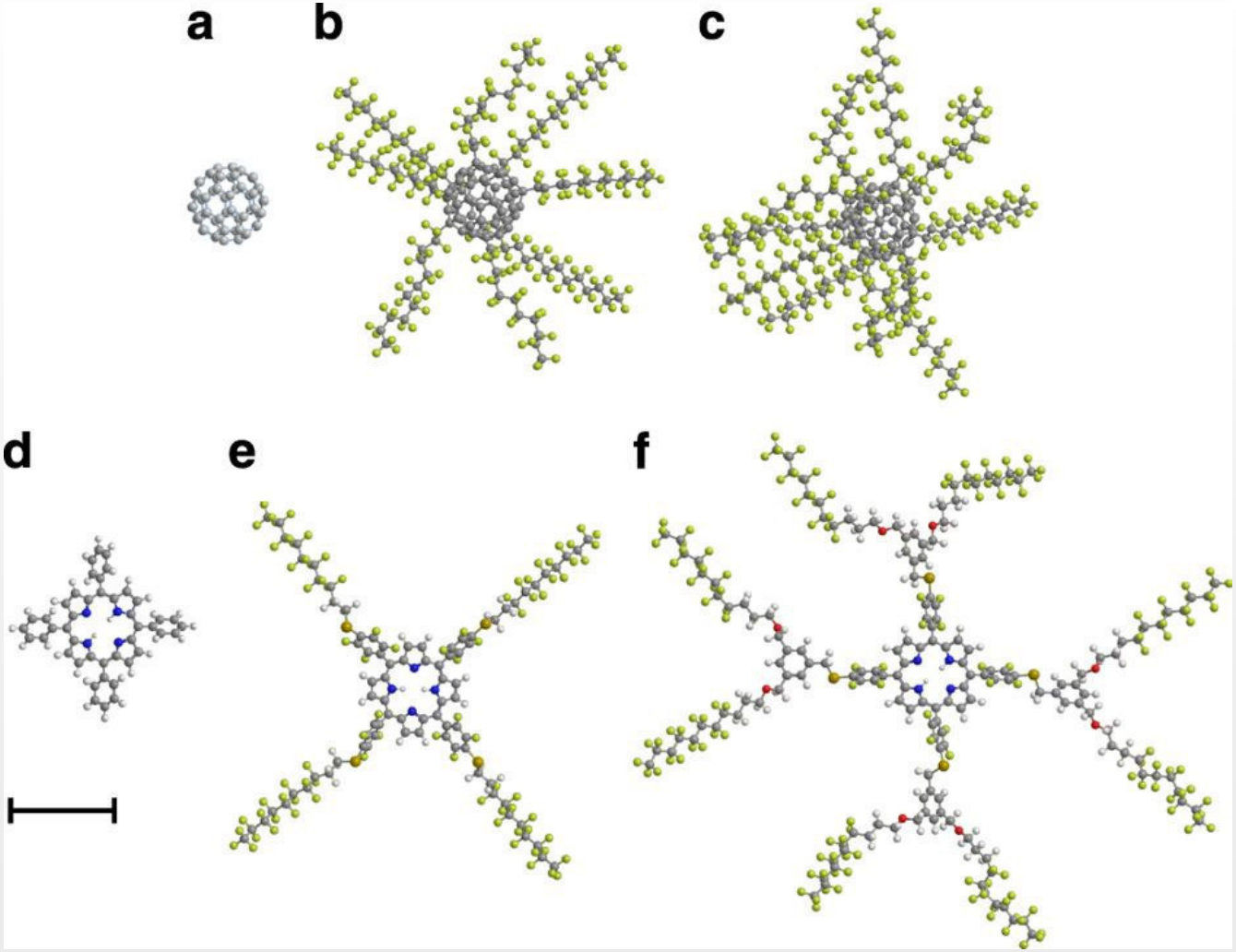

The Schroedinger‘s cat

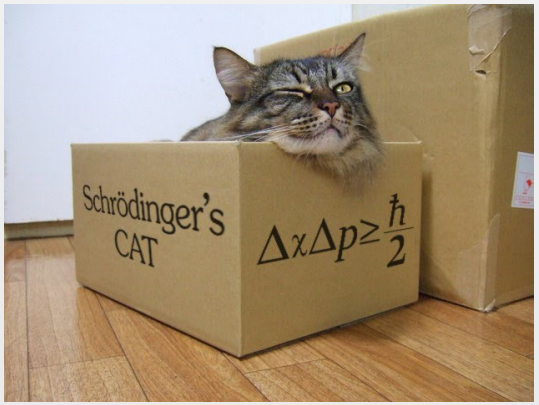

$$|\Psi\rangle = \frac{|\text{cat}\rangle + |\text{dead cat}\rangle}{\sqrt{2}}$$

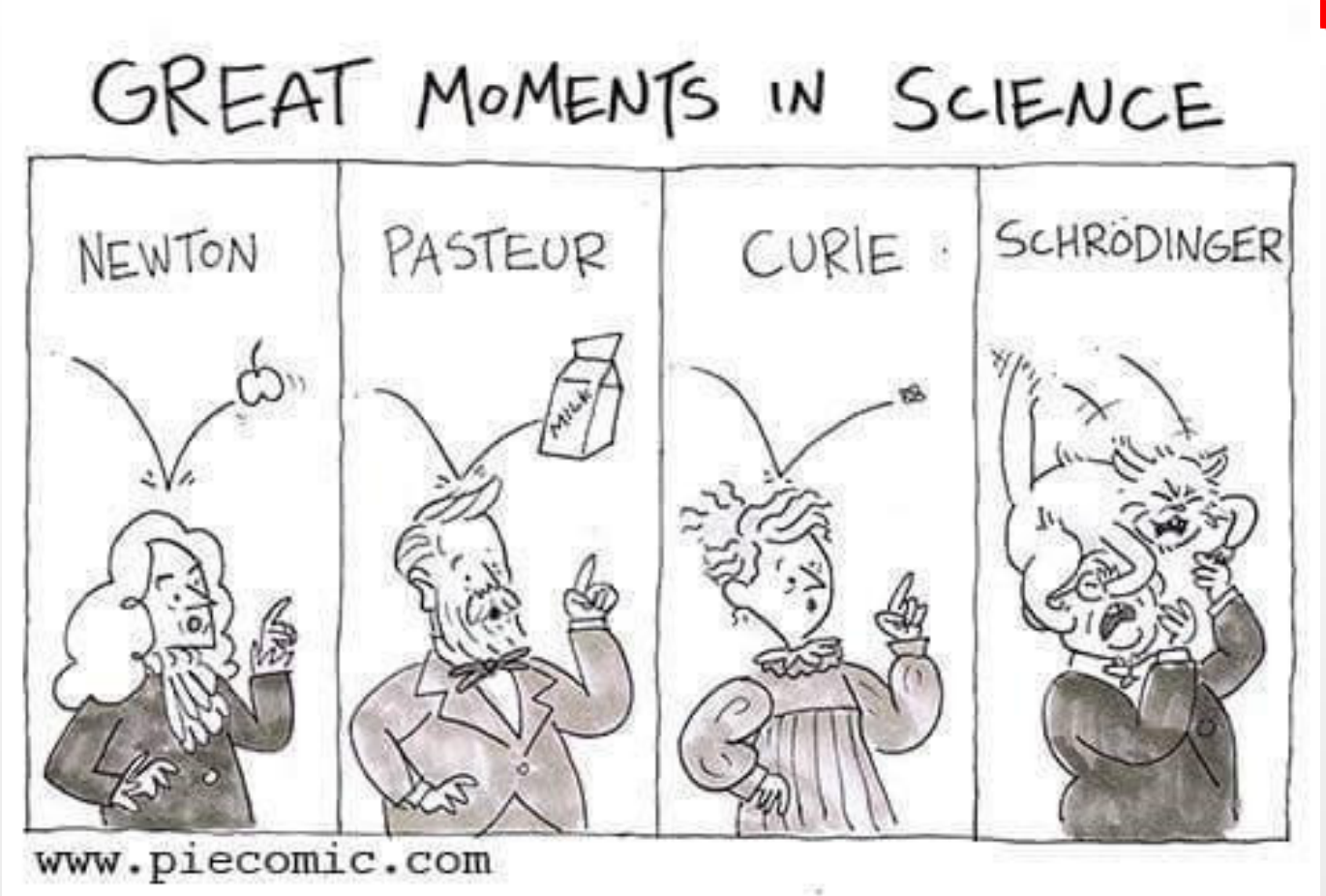
GREAT MOMENTS IN SCIENCE
NEWTON
PASTEUR
CURIE
SCHRÖDINGER
MILK
www.piecomic.com

Many-world scenario of Quantum Mechanics

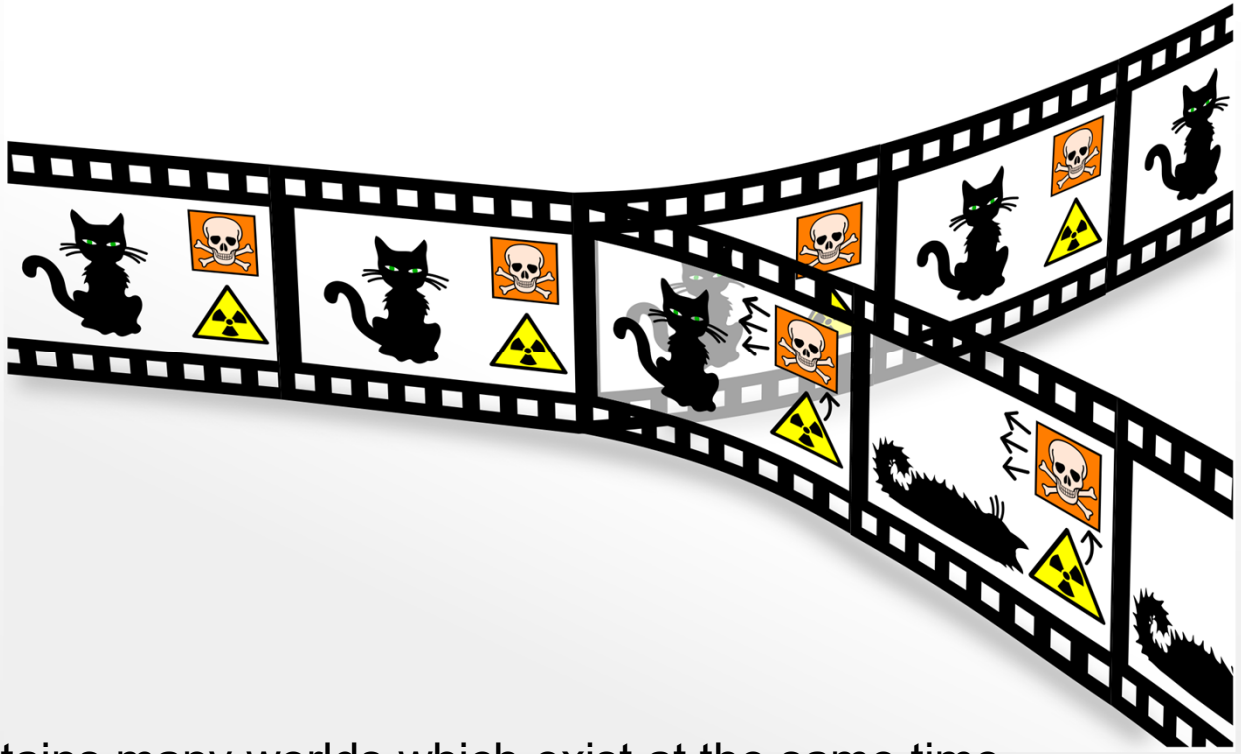

Ψ contains many worlds which exist at the same time.

H. Everett, Rev. Mod. Phys. 29 (1957) 454.
J. A. Wheeler, Rev. Mod. Phys. 29 (1957) 463
DeWitt Bryce S, Physics Today, Vol. 23, No. 9 (1970)

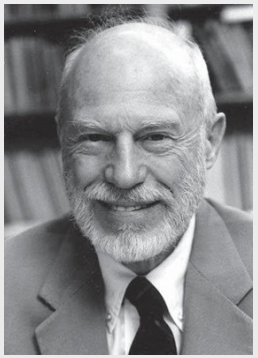

Love and quantum

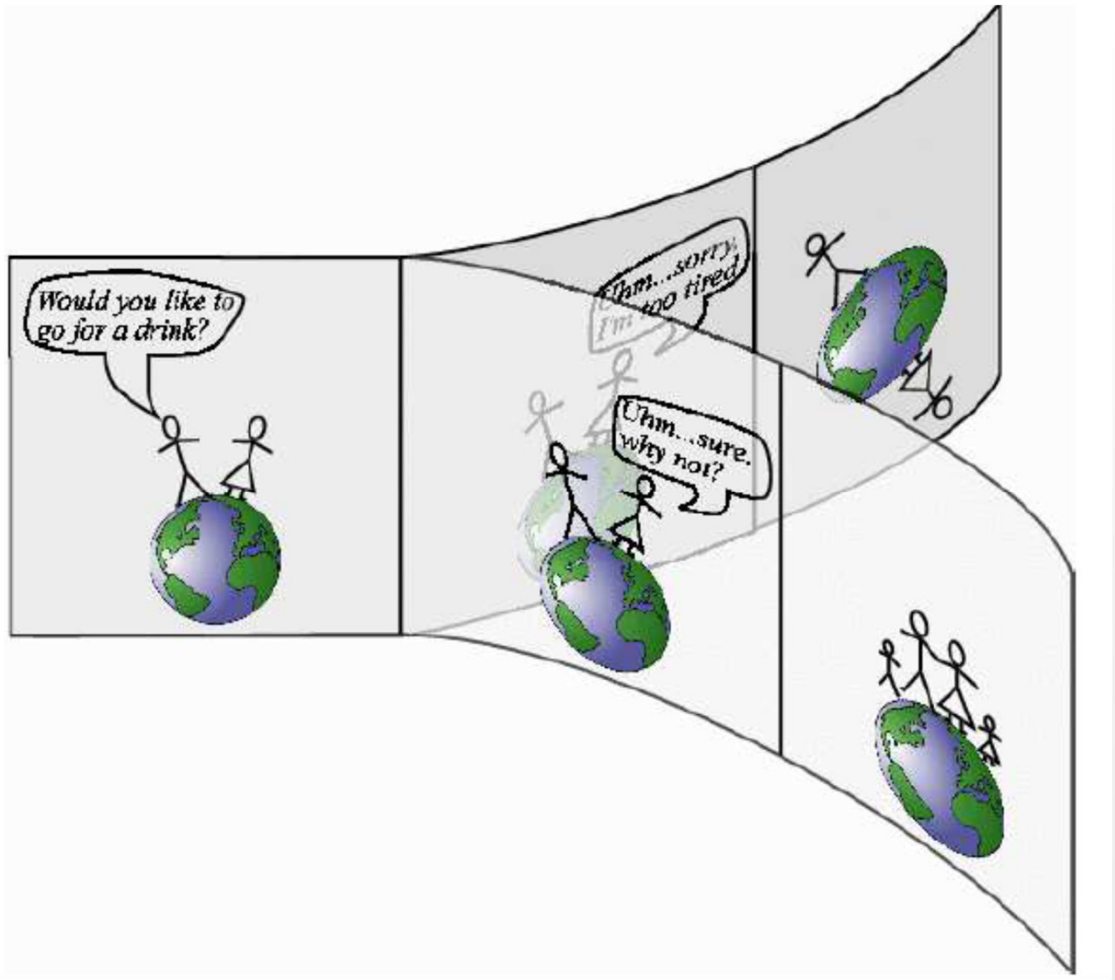

QM and philosophy, a strong connection
(yet, we shall reject the so-called quantum mystic)

More and more worlds

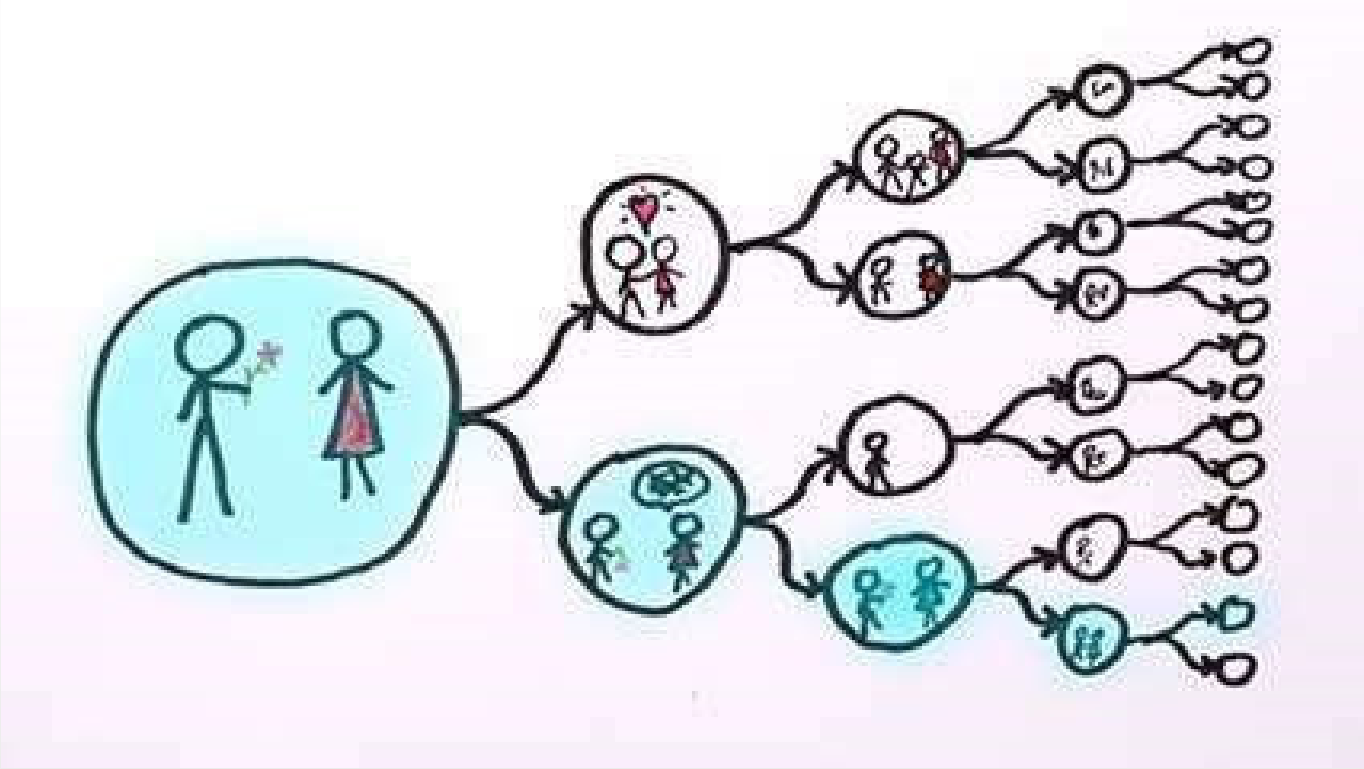

Applications of QM

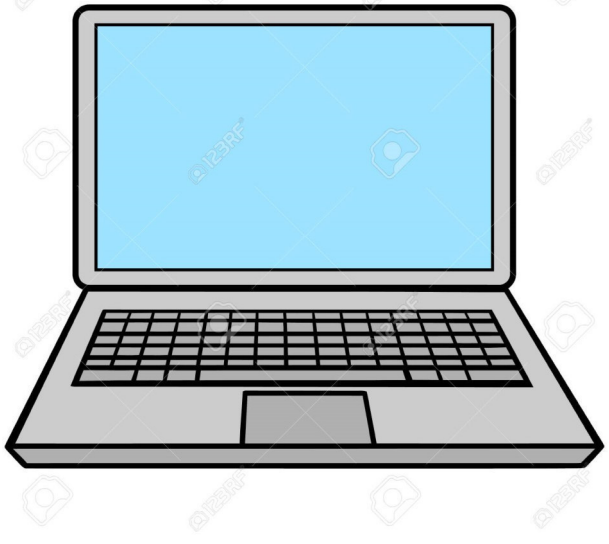

Applications of QM

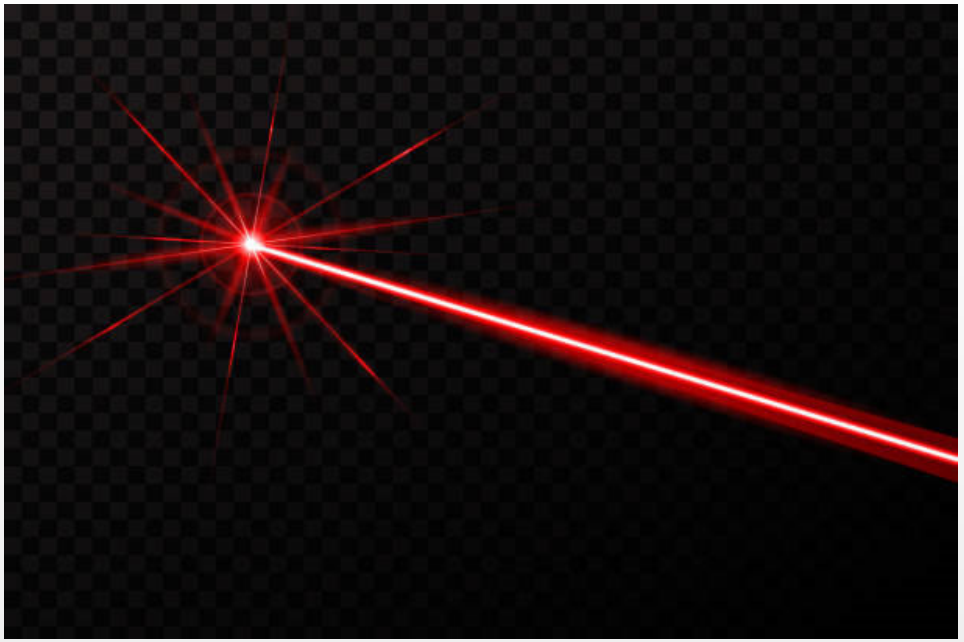

Applications of QM

Generation of genuine random numbers is very important in many numerical applications (including physics, finance, …)

‘God does not play dices’ (A. Einstein)

‘Indeed, it seems that IT does’

Radiation cancer therapy

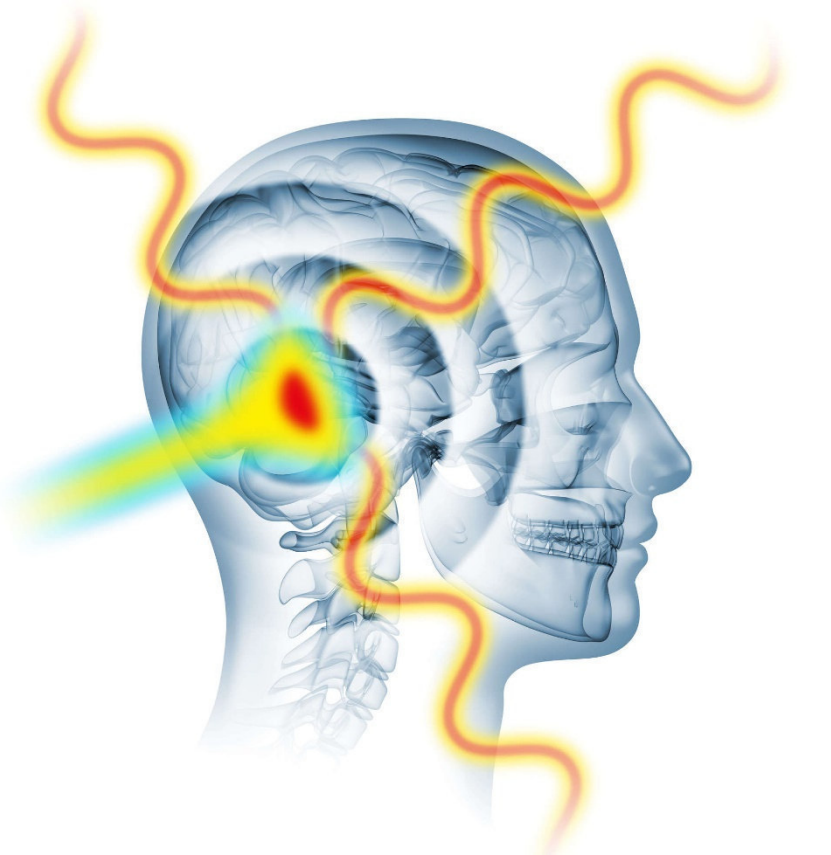

Bombarding cancer with particles
such as photons, electrons,
But also protons, atomic nuclei, …

QM at work in medicine

PET

Positron Emission Tomography

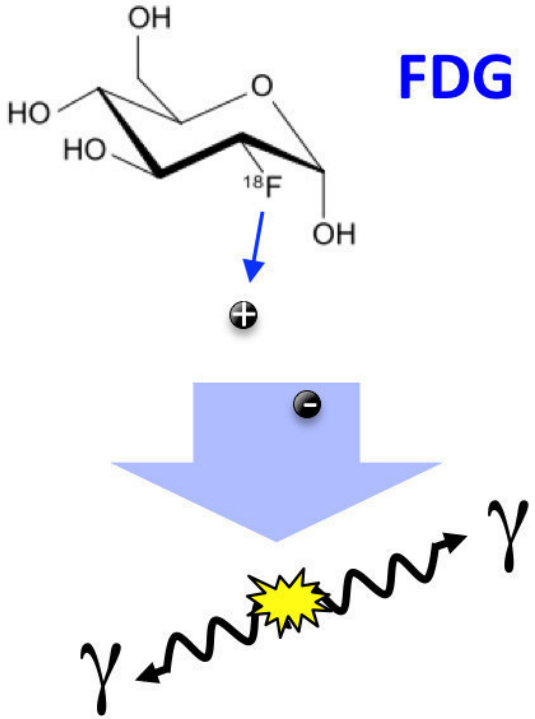

It makes use of anti-matter!

MRI: magnetic resonance imaging

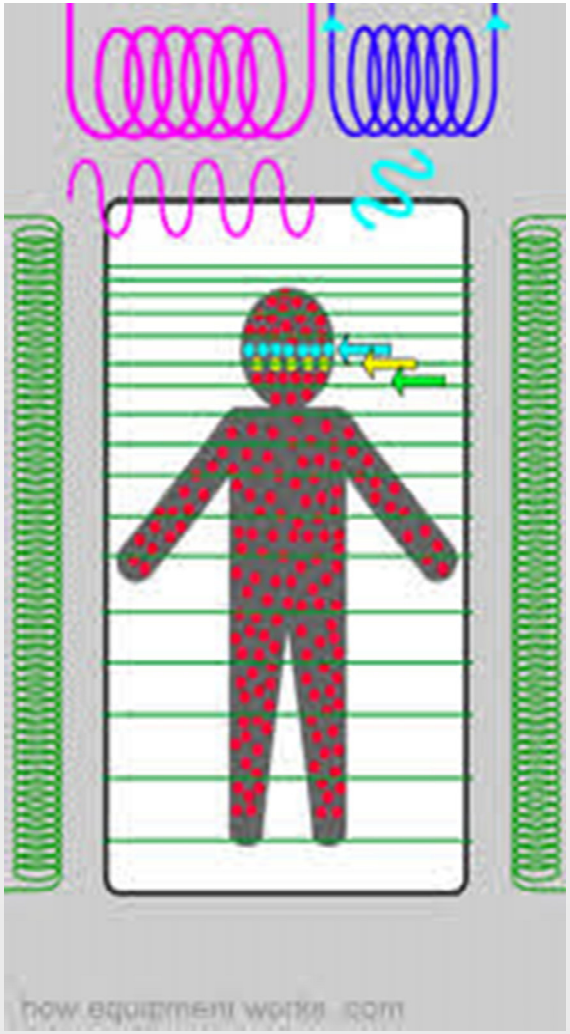

Pulse oximetry

It uses photelectric sensors (based on the Einstein Nobel price's discovery,…), diode, and absorption of light.

Quantum chemistry

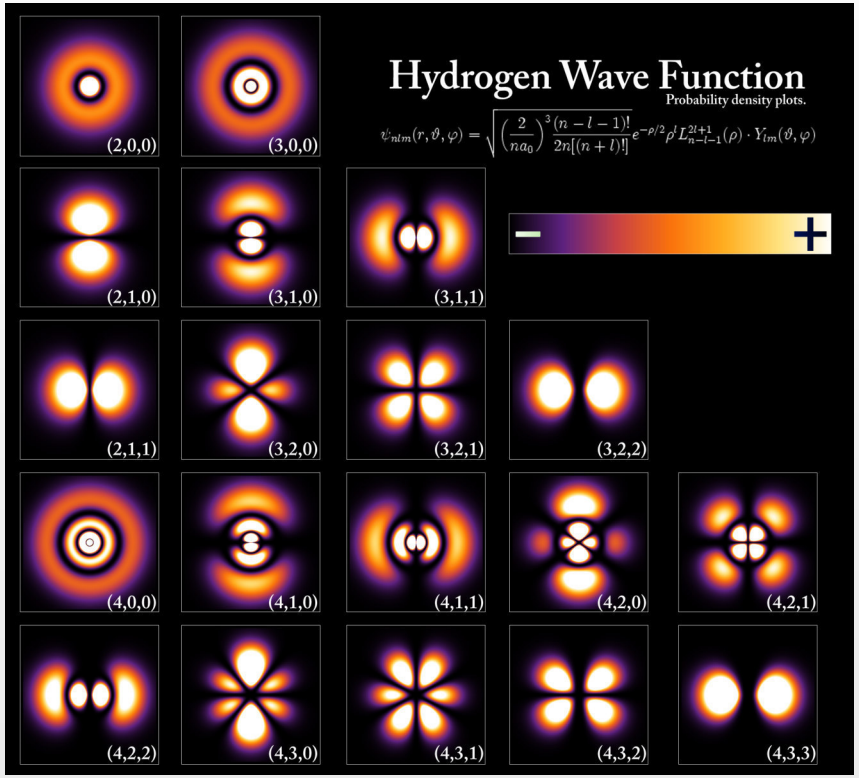

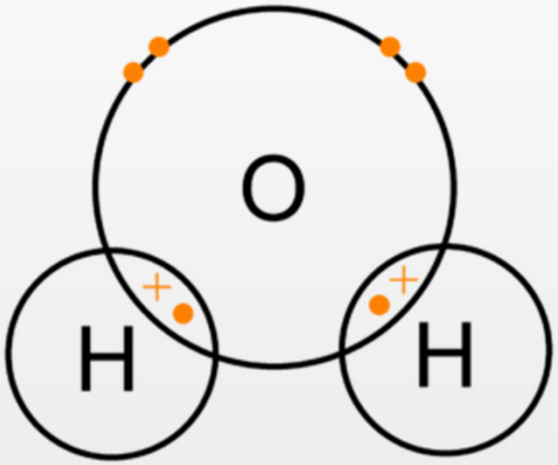

Quantum biology

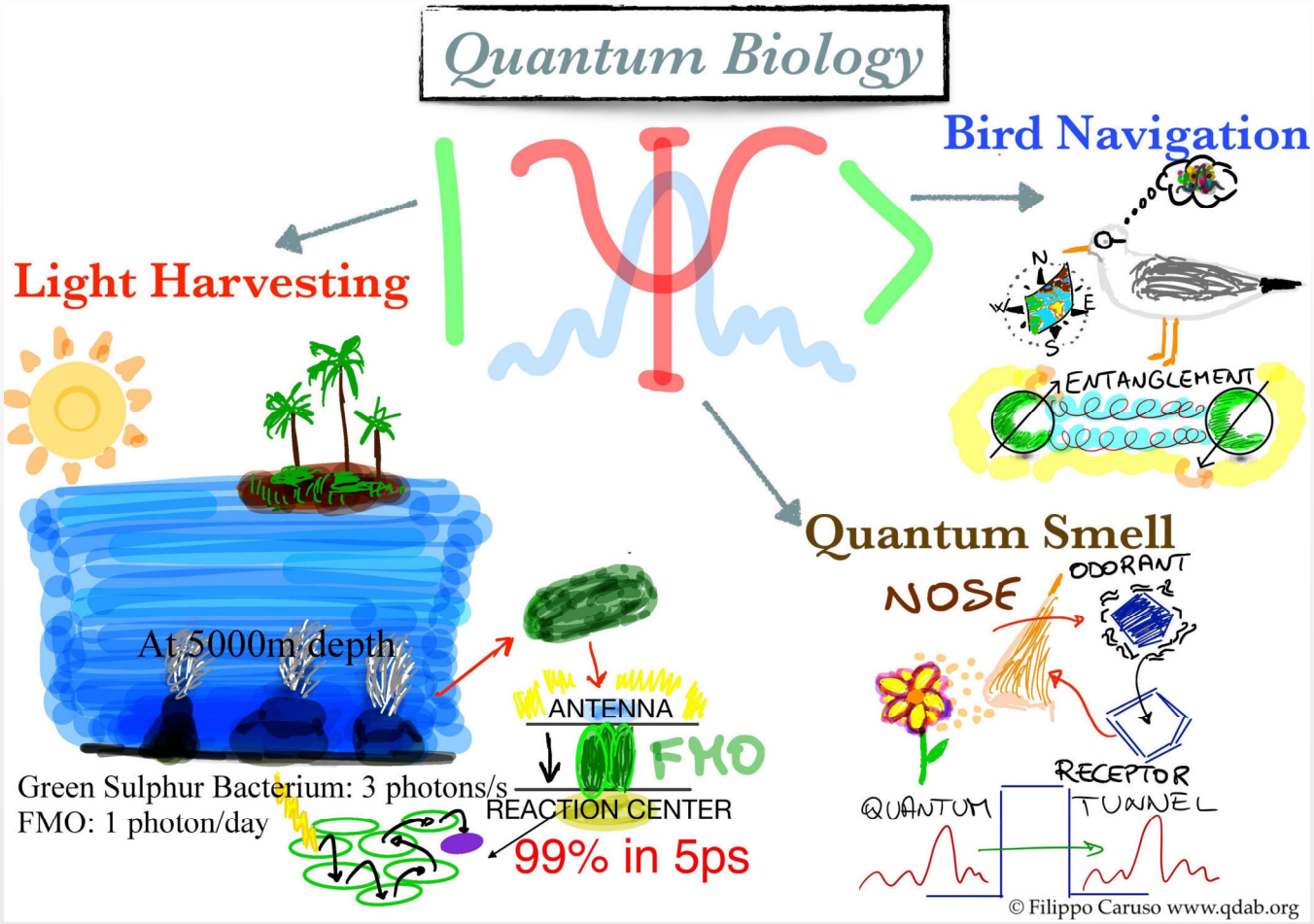

https://www.lindau-nobel.org/what-is-quantum-biology/

A very peculiar QM effect: Tunnel

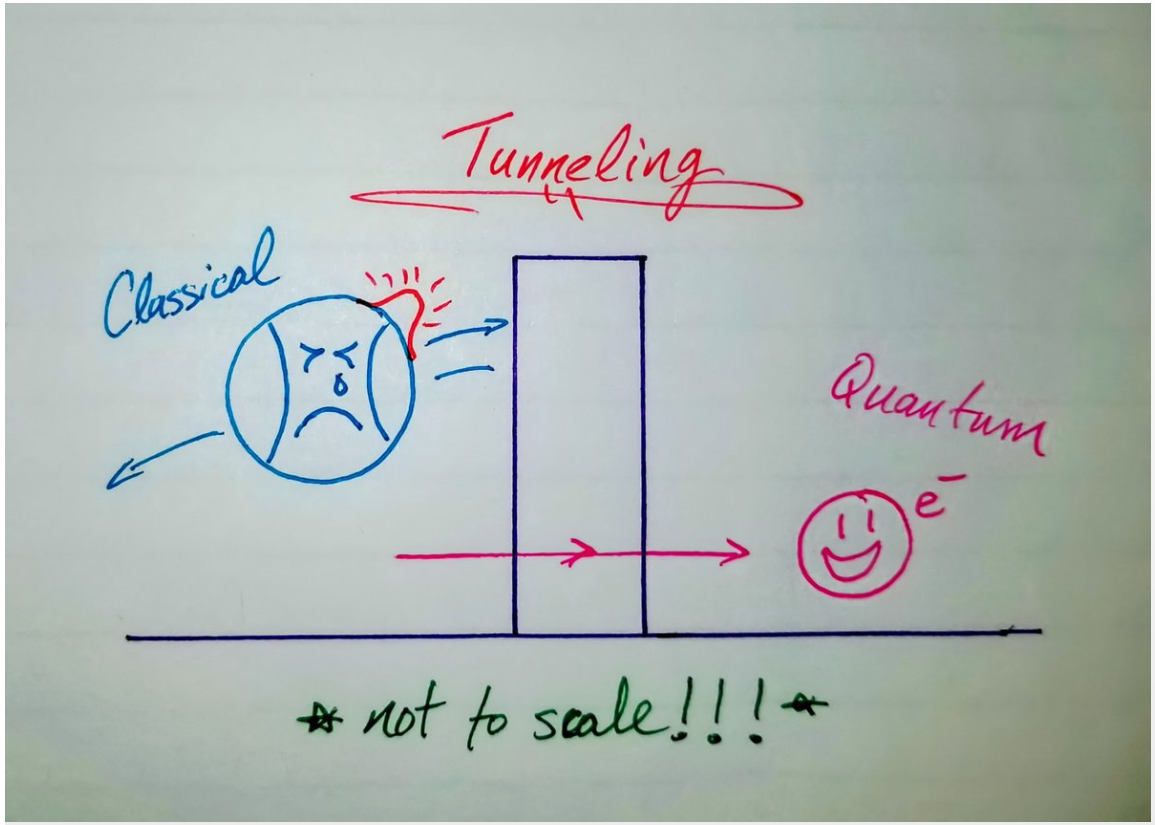

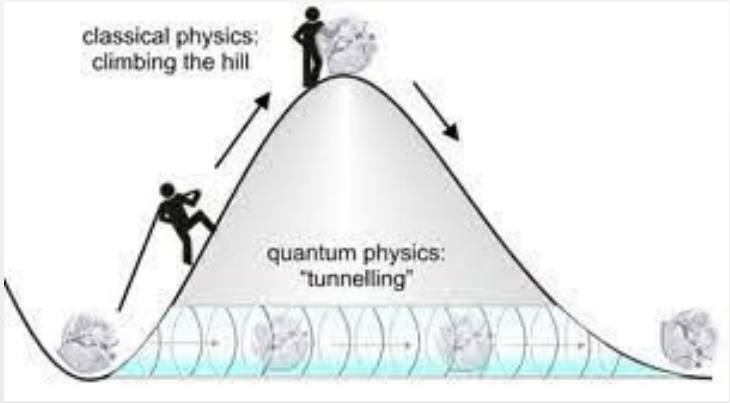

Two examples involving tunneling and UJK

Contents lists available at ScienceDirect

Nuclear Instruments and Methods in Physics Research B

journal homepage: www.elsevier.com/locate/nimb

Modification of gold and titanium nanolayers using slow highly charged Xe^{q+} ions

I. Stabrawa [a,b], D. Banaś [a,b,*], A. Kubala-Kukuś [a,b], K. Szary [a], J. Braziewicz [a], J. Czub [a], Ł. Jabłoński [a], P. Jagodziński [c], D. Sobota [a], M. Pajek [a], K. Skrzypiec [d], E. Mendyk [d], M. Teodorczyk [e]

[a] Institute of Physics, Jan Kochanowski University, Świętokrzyska 15, 25-406 Kielce, Poland

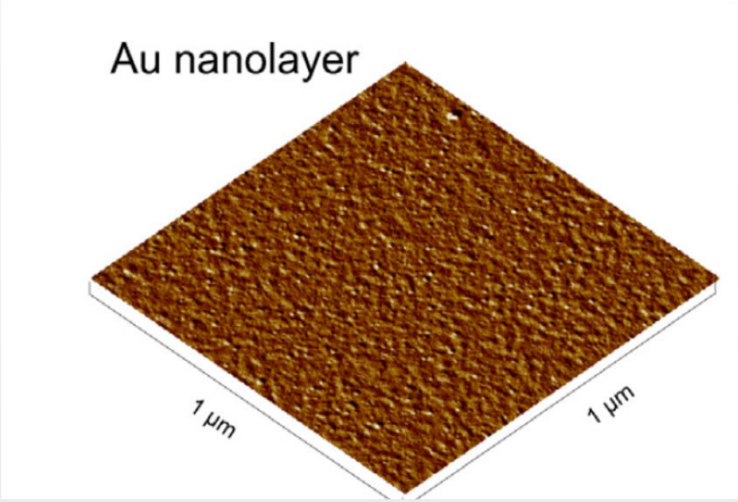

PHYSICAL REVIEW A 102, 022204 (2020)

Capturing nonexponential dynamics in the presence of two decay channels

Francesco Giacosa [1,2], Przemysław Kościk [3], and Tomasz Sowiński [4]

[1] Institute of Physics, Jan-Kochanowski University, ulica Uniwersytecka 7, PL-25406 Kielce, Poland

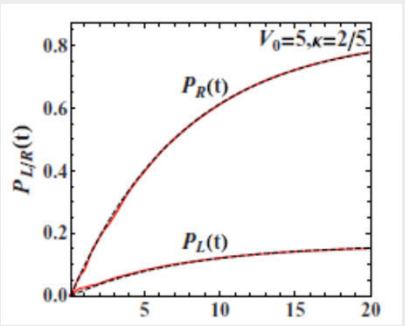

From computers to quantum computers

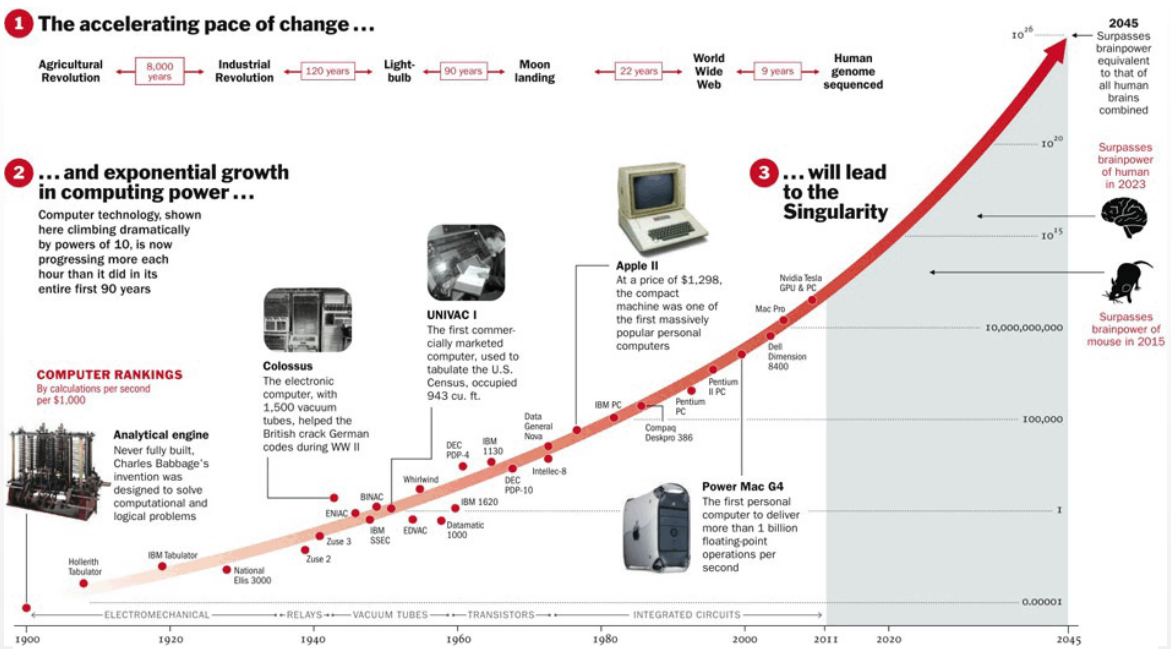

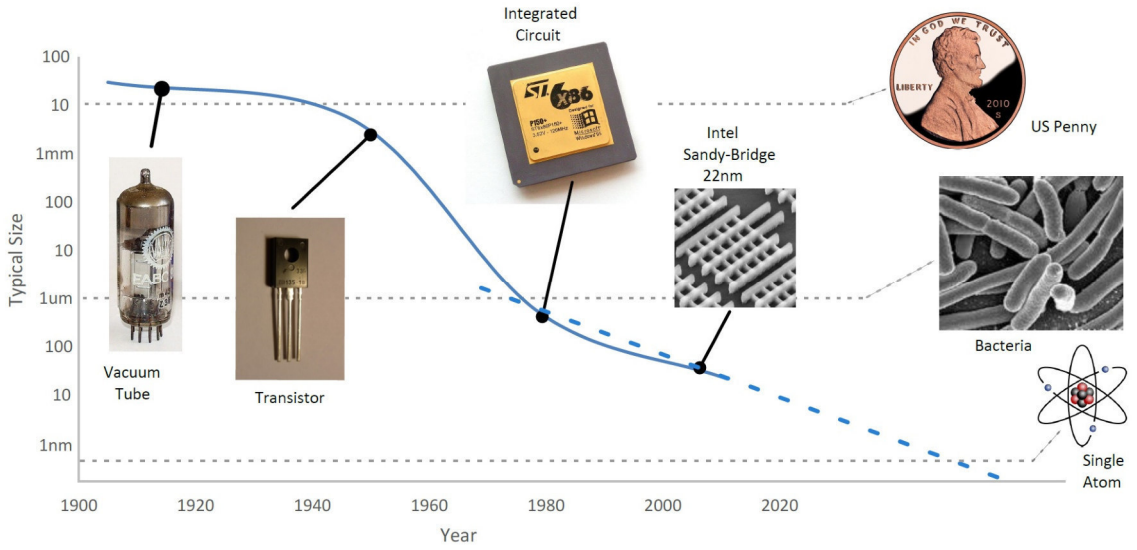

Quantum computing

Bit versus Qubit

Bit

„0“ or „1“

Qubit

„0“ and „1“

Superposition

Qubits

amplitudes

0	a_0
1	a_1

$$|\psi\rangle = a_0|0\rangle + a_1|1\rangle$$

a_i *is a complex number*

Schrödinger's Cat

$$\frac{1}{\sqrt{2}}\left(\left|\right.\right.$$  $$\left.\left.\right\rangle + \left|\right.\right.$$  $$\left.\left.\right\rangle\right)$$

Use of qubits: quantum simulations and quantum cryptography

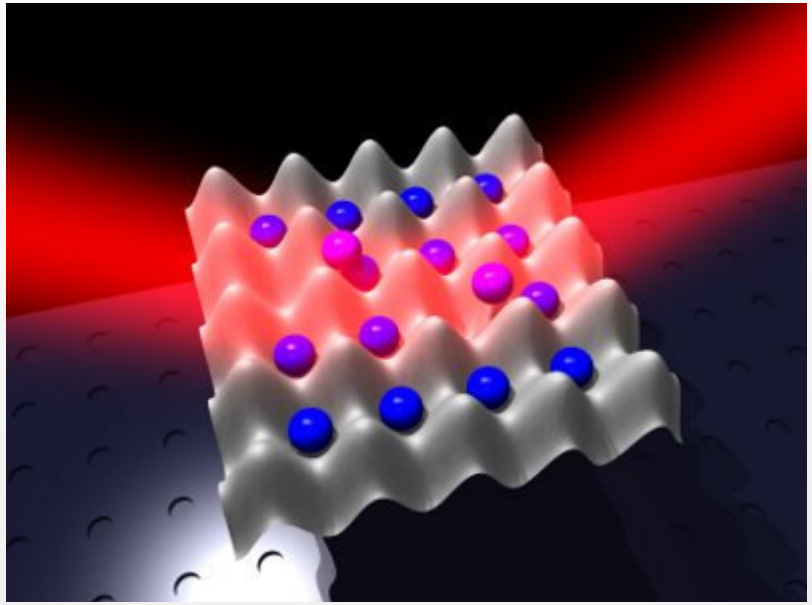

www.lens.unifi.it

Ultracold atoms trapped in optical lattices can be the material base for two kind of calculator: quantum computers and quantum simulators.

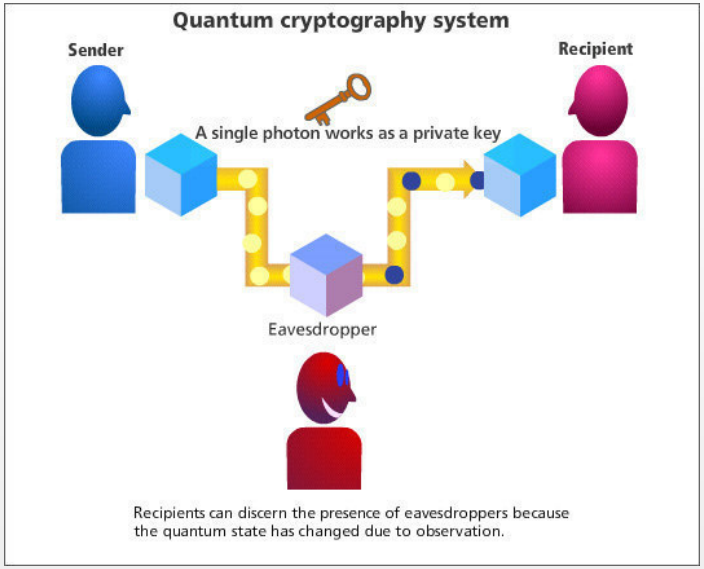

The importance of sending information is immense.

The quantum computer race

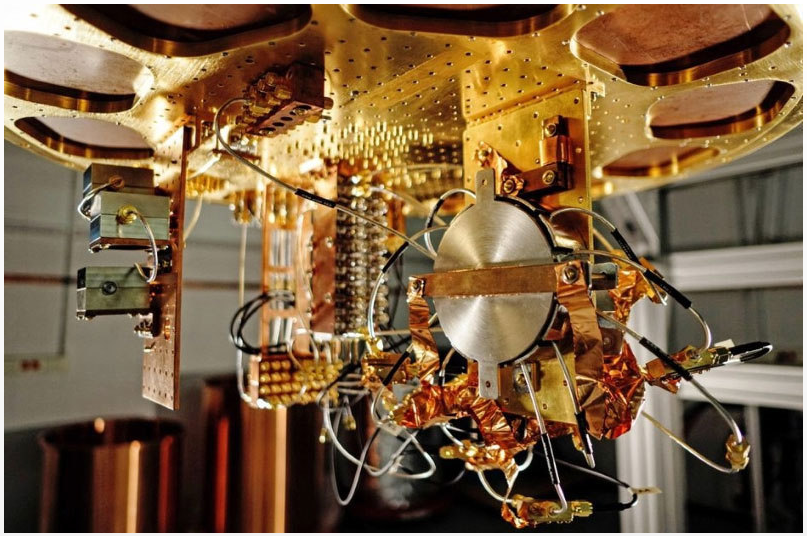

In 2019 the first announcement of quantum supremacy

Quantum computers can factorize into prime numbers!
This brings us back to the beginning of the talk!

How to calculate derivtives

Quantum Information and Computation, Vol. 21, No. 1&2 (2021) 0080-0094

QUANTUM ALGORITHMIC DIFFERENTIATION

The figure below shows the corresponding quantum circuit:

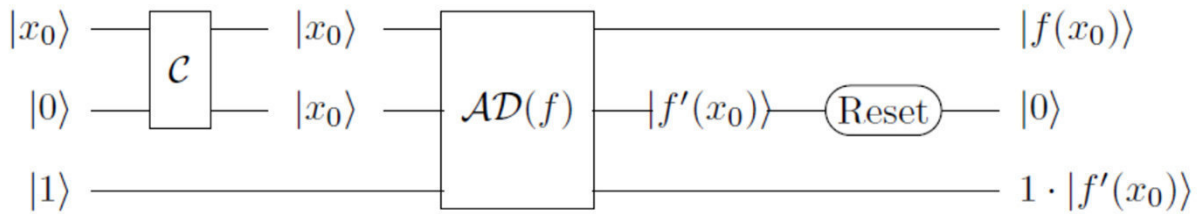

For more discussion on all these topics

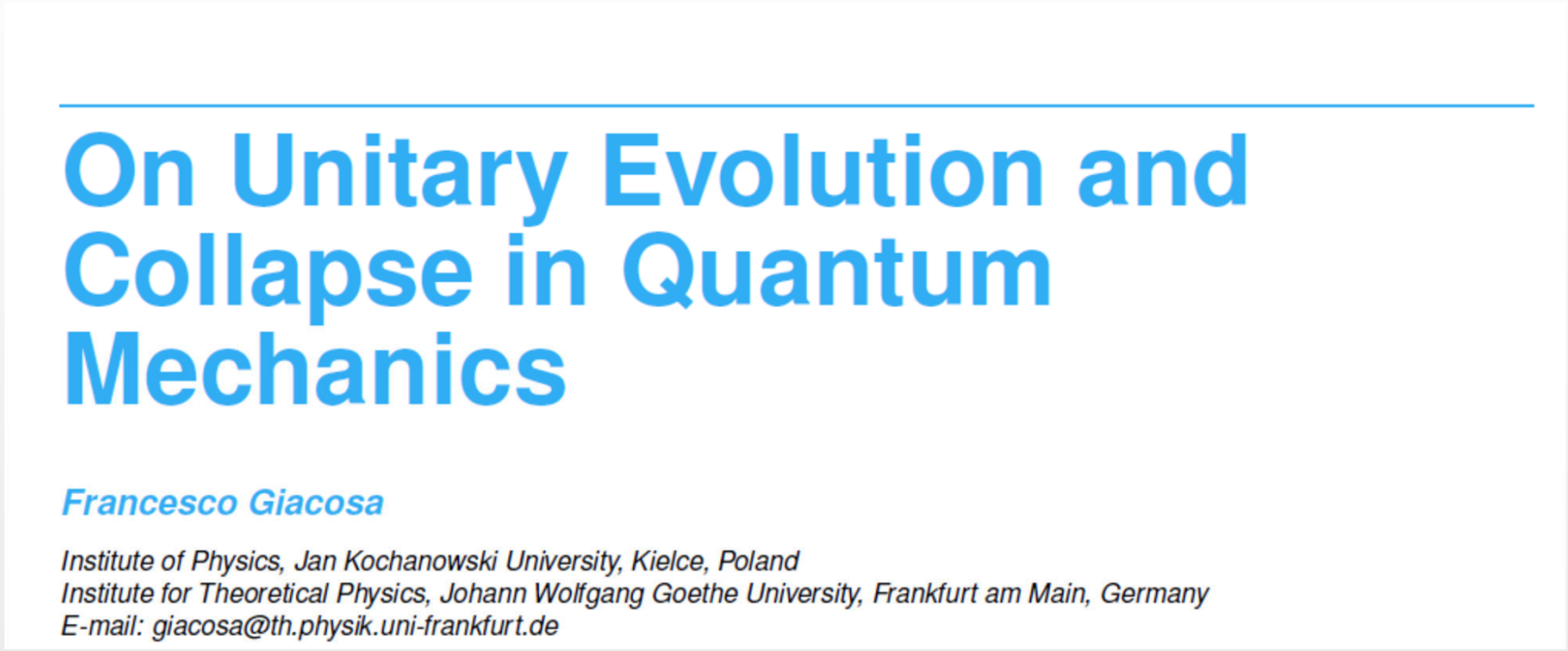

On Unitary Evolution and Collapse in Quantum Mechanics

Francesco Giacosa

Institute of Physics, Jan Kochanowski University, Kielce, Poland
Institute for Theoretical Physics, Johann Wolfgang Goethe University, Frankfurt am Main, Germany
E-mail: giacosa@th.physik.uni-frankfurt.de

http://quanta.ws/ojs/index.php/quanta/article/view/26/92
https://arxiv.org/abs/1406.2344

Concluding remarks

- Scientific disciplines are interconnected (in this sense our school works)
- If you understanding something, this is (i) interesting on its own and (ii) it will be most probably useful in the future. Just do your job as best as you can.
- Importance of science against pseudoscience.
- PhDs are crucial for any University.

3. Publications from 1/10/2019 to 30/9/2021

(besides the already published ones, you may add to the list also those articles accepted but not yet appeared in the journals and also articles sent to the journal under the revision process. In the last cases, put a proof (email, screen-shot,…) about the status of those papers and add the pdf in the end.

Published papers

1) S. Samanta and F. Giacosa,
QFT treatment of a bound state in a thermal gas,
Phys. Rev. D 102 (2021) no.11, 116023
doi:10.1103/PhysRevD.102.116023
[arXiv:2009.13547 [hep-ph]].

2) G. Colucci and F. Giacosa
Quantum algorithmic differentiation
Quantum Information and Computation, Vol. 21, No. 1&2 (2021) 0080-0094
DOI: 10.26421/QIC21.1-2
[arXiv:2006.13370 [quant-ph]].

3) F. Giacosa, P. Kościk and T. Sowiński,
Capturing non-exponential dynamics in the presence of two decay channels,
Phys. Rev. A 102 (2020) no.2, 022204
doi:10.1103/PhysRevA.102.022204
arXiv:1912.06394 [quant-ph].

4) W. I. Eshraim, C. S. Fischer, F. Giacosa and D. Parganlija,
Hybrid phenomenology in a chiral approach,
Eur. Phys. J. Plus \textbf{135} (2020) no.12, 945
DOI:10.1140/epjp/s13360-020-00900-z
arXiv:2001.06106 [hep-ph].

5) F. Giacosa and G. Pagliara,
Measurement of the neutron lifetime and inverse quantum Zeno effect,
Phys. Rev. D 101 (2020) no.5, 056003
DOI: 10.1103/PhysRevD.101.056003
[arXiv:1906.10024 [hep-ph]].

6) F. Giacosa,
QZE and IZE in a simple approach and the neutron decay,
Proceedings, 26th Cracow Epiphany Conference on LHC Physics: Standard Model and Beyond (Epiphany), 7-10/1/2020, Krakow, Poland.
Acta Phys. Polon. B 51 (2020), 1345
doi:10.5506/APhysPolB.51.1345
[arXiv:2004.07772 [hep-ph]].

7) F. Giacosa,
The Lee model: a tool to study decays,
Proceedings of the symposium 'symmetries in science' , 4-9/8/2019, Bregenz, Austria.
J. Phys. Conf. Ser. 1612 (2020) no.1, 012012
doi: 10.1088/1742-6596/1612/1/012012
arXiv:2001.07781 [hep-ph].

8) F. Giacosa,
Modelling the inverse Zeno effect for the neutron decay,
Proceedings of 3rd Jagiellonian Symposium on Fundamental and Applied Subatomic Physics (J-SYMPOSIUM 2019) 24-28 June 2019. Kraków, Poland
Acta Phys. Polon. B 51 (2020) 77
DOI: 10.5506/APhysPolB.51.77
[arXiv:1909.01099 [hep-ph]].

9) F. Giacosa,
Companion poles: from the $a_{0}(980)$ to the $X(3872)$,
Proceedings of the 11th International Winter Workshop "Excited QCD" 2019 30 Jan - 03 Feb 2019. Schladming, Austria
Acta Phys. Polon. Supp. 13 (2020) 83
DOI: 10.5506/APhysPolBSupp.13.83
[arXiv:1904.10368 [hep-ph].]

10) F. Giacosa, M. Piotrowska and S. Coito,
$X(3872)$ as virtual companion pole of the charm-anticharm state $\chi_{c1}(2P)$,
Int. J. Mod. Phys. A 34 (2019) no.29, 1950173

DOI: 10.1142/S0217751X19501732
arXiv:1903.06926 [hep-ph].

11) S. Coito and F. Giacosa,
On the origin of the $Y(4260)$,
Acta Phys. Polon. B 51 (2020) no.8, 1713-1737
doi:10.5506/APhysPolB.51.1713
arXiv:1902.09268 [hep-ph].

Papers under the revision process

1) F. Giacosa and G. Pagliara,
Leggett-Garg inequalities and decays of unstable systems,
Submitted to Phys. Rev. A
[arXiv:2104.04398 [quant-ph]].

See the pdf in the end

4. Participation & talks/posters at scientific conferences

1) Talk for Light-and heavy-quark hadron spectroscopy, Horizon 2020 research and innovation programme (STRONG-2020) JRA7-HaSP, online meeting, 15-17/12/2020, http://www.strong-2020.eu/joint-research-activity/jra7-hasp.html http://ific.uv.es/nucth/TH-WP25-H2020/ https://indico.ice.csic.es/event/24/

Title: **Hybrid decays in a chiral approach**

2) Invited talk prepared for Excited QCD 2020, 2-8/2/2020 – Krynica Zroj – Poland https://indico.cern.ch/event/827578/overview :

Title: **Hybrids in a chiral approach**

3) Talk prepared for Epiphany conference 2020: LHC physics: standard model and beyond IFJ PAN Krakow 7-10/1/2020, https://indico.cern.ch/event/819524/

Title: **Neutron decay anomaly: hint to BSM physics, a QM effect, or just a systematic error?**

4) Invited talk for Talk for the 45. Zjazd Fizyków Polskich, 13-18/9/2019, Krakow, Poland http://www.45zfp.uj.edu.pl/#/

Title: **Glueballs and hybrids below 2.6 GeV.**

Proof of participation/talks/posters at conferences

(it can be email, screenshots, participation attests, etc.) Put the link of the webpages (see above). Below I put two as examples

1)

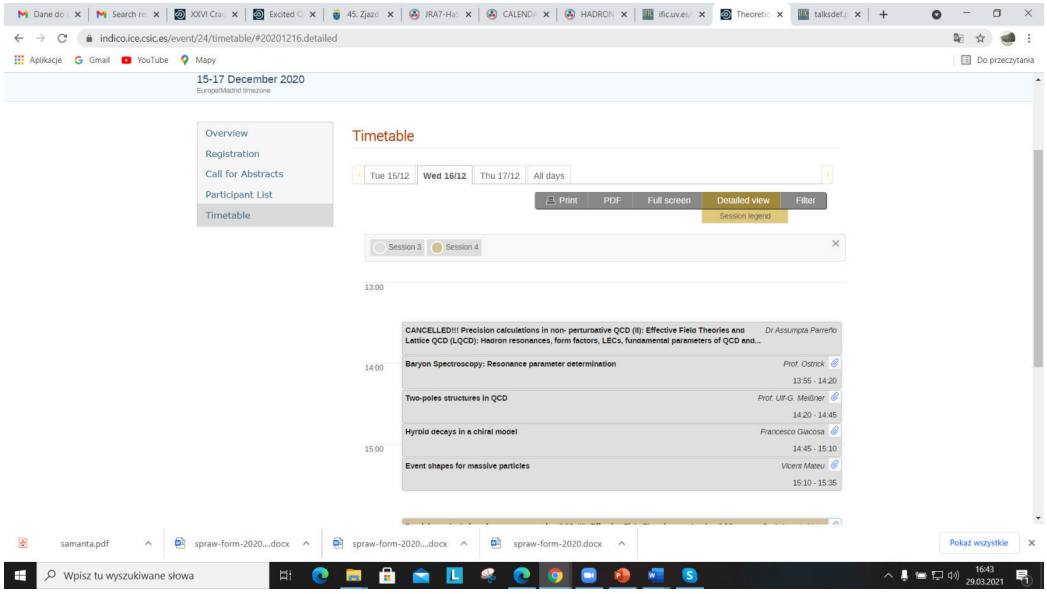

2)

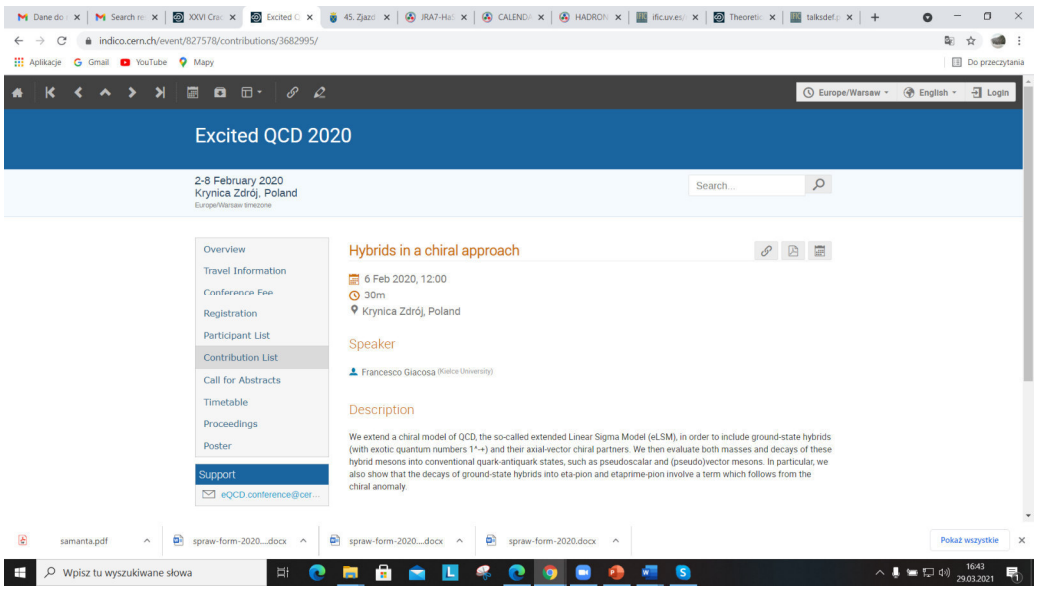

5. Seminars at Universities/Institutes

1) Title: **Is there a problem with the lifetime of the neutron?**
Talk prepared for the Institute's seminar
Institute of Physics, UJK, Kielce, 4/3/2020.

2) Title: **Not every peak nor every pole is necessarily a resonance: some case studies**
Invited talk prepared for the AGH – High Energy Physics Seminar,
AGH University, Kraków, Poland, 22/11/2019

3) Title: **Phenomenological aspects of the axial anomaly.**
Invited talk at the theory seminar of the IFJ PAN of Krakow, 21/11/2019

Proofs

(it can be email, an active link, …)

Below I put 2 as an example:

2) http://www.ftj.agh.edu.pl/koidc/materials/seminaria/22112019-FrancescoGiacosa-Resonances.pdf

6. Scientific internships

Put here your scientific internships (at least 14 days) .

Where, how long, some doc proving it.

7. Co-organization of conferences

Put below the conferences which you helped to co-organize and, if available, a link to the web-page of the conference

1) Support in the organization of the PhD forum 2020 at the UJK, 17-19/11/2020, Kielce, UJK (via zoom and teams) https://forumdoktorantow.ujk.edu.pl/

8. Grants

1) OPUS project 2019/33/B/ST2/00613 od Polish National Science Centre (NCN)
   Title: Znaczenie symetrii i anomalii QCD w fenomenologii mezonów
   Start: 17/2/2020; Planned end: 16/2/2024
   PI: prof. dr hab. Francesco Giacosa
   https://projekty.ncn.gov.pl/index.php?projekt_id=444770

2) Minigrant UJK (rok 2020): SMGR.RN.20.223.629
   Title: Scattering of bosons in the vacuum and at nonzero temperature
   Start: 1/1/2020, End: 30/4/2021
   PI: prof. dr hab. Francesco Giacosa.

9. Query

Put here query (kwerendy).

Where, how long, some doc proving it.

10. Other activities

(including organizational activities, popularization, additional courses)

1) Organization activities: Director of the PhD School of the UJK exactly since 1/10/2020😊

2) Title: Quarks
   Wykład Otwarty UJK, prelegent prof. dr hab. Francesco Giacosa, 5/11/2020
   https://www.youtube.com/watch?v=xjXjGu6JE3g&t=1553s

3) ***Profesor dr hab. Francesco Giacosa – gość koła naukowego „Ciekawi świata***" SP1 BUSKO 26/11/2020
   http://psp1busko.szkolnastrona.pl/art,331,profesor-dr-hab-francesco-giacosa-gosc-kola-naukowego-ciekawi-swiata

4) Title: Co Włosi mowią rękami?
   Francesco Giacosa, Uniwersytet Dziecięcy Jana Kochanowskiego w Kielcach, 15.2.2020:

5) Title: Fascynujące technologie fizyczne
   Uniwersytet Dziecięcy Jana Kochanowskiego w Kielcach, 21.12.2019:

11. pdf of your publications

Pdf of the publications
(put in the following all your publications)

Note, I put only 2 as an example

QFT treatment of a bound state in a thermal gas

Subhasis Samanta[1] and Francesco Giacosa[1,2]

[1]*Institute of Physics, Jan-Kochanowski University, ul. Swietokrzyska 15, 25-406, Kielce, Poland*
[2]*Institute for Theoretical Physics, J. W. Goethe University, Max-von-Laue-Str. 1, 60438 Frankfurt, Germany*

(Received 1 October 2020; accepted 8 December 2020; published 31 December 2020)

We investigate how to include bound states in a thermal gas in the context of quantum field theory (QFT). To this end, we use for definiteness a scalar QFT with a φ^4 interaction, where the field φ represents a particle with mass m. A bound state of the φ-φ type is created when the coupling constant is negative and its modulus is larger than a certain critical value. We investigate the contribution of this bound state to the pressure of the thermal gas of the system by using the S-matrix formalism involving the derivative of the phase-shift scattering. Our analysis, which is based on an unitarized one-loop resumed approach which renders the theory finite and well defined for each value of the coupling constant, leads to the following main results: (i) We generalize the phase-shift formula in order to take into account within a unique formal approach the two-particle interaction as well as the bound state (if existent). (ii) *On the one hand*, the number density of the bound state in the system at a certain temperature T is obtained by the standard thermal integral; this is the case for any binding energy, even if it is much smaller than the temperature of the thermal gas. (iii) *On the other hand*, the contribution of the bound state to the total pressure is partly—but not completely—canceled by the two-particle interaction contribution to the pressure. (iv) The pressure as a function of the coupling constant is *continuous* also at the critical coupling for the bound state formation: the jump in pressure due to the sudden appearance of the bound state is exactly canceled by an analogous jump (but with opposite sign) of the interaction contribution to the pressure.

DOI: 10.1103/PhysRevD.102.116023

I. INTRODUCTION

Measurement of bound states, such as deuteron (d), helium-3 (^{3}He), tritium (^{3}H), helium-4 (^{4}He), hypertritium ($^3_\Lambda$H) and their antiparticles, was reported in high energy proton-proton, proton-nucleus (pA) and nucleus-nucleus (AA) collisions [1–7]. Moreover, the QCD spectrum has also revealed the existence of a whole new class of X, Y, and Z resonances that are not predicted by the quark model, some of which can be mesonic molecular bound states; see e.g., Ref. [8] and references therein. Last but not least, also pentaquark states [9] can be understood as molecular objects.

The production of nuclei as well as other hadronic bound states has attracted a lot of interest because their binding energies are typically much smaller than the temperature realized in high energy collisions, hence at the first sight it is quite puzzling that such objects can form in such a hot environment. In addition, light nuclei are also potential candidates to search for the critical point in the quantum chromodynamics (QCD) phase diagram [10–13]. Excess production of some light antinuclei in cosmic rays and dark matter experiments [14–16] has also been investigated.

There are several models, notably thermal models [17–22], nucleon coalescence models [11,23–33], and dynamical models [34,35] which aim to explain the production of bound states in high energy collisions. Yet, there are differences among them, and it is not yet clear up to now which approach is the correct one. In other words, are bound states produced according to their statistic distribution at temperature T? If yes, which is their contribution to the pressure?

In the present work, we intend to answer these questions in the context of Quantum Field Theory (QFT). To this end, we use the well known scalar φ^4-interaction, where φ is a field with mass m.

First, we evaluate the scattering phase shift at tree level and at the one-loop resumed level. In the latter (and necessary) step, we choose a proper unitarization scheme at the resumed one-loop level for which (i) no new energy scale appears and (ii) the results are finite and well defined for any value of the coupling constant, denoted as λ (the corresponding potential reads $V = \lambda^4\varphi^4/4!$).

When $\lambda > 0$ the interaction is repulsive, and the phase shift is always decreasing with the increase of the running

energy $\sqrt{s}$ and smaller than zero. When $\lambda < 0$ (and its modulus is smaller than a certain critical value denoted as λ_c) the interaction is attractive and the phase shift is positive, rising for small $\sqrt{s}$ and decreasing afterward. Yet, when $\lambda < \lambda_c < 0$, a bound state is formed, whose mass is exactly equals to $2m$ for $\lambda = \lambda_c$ and is smaller than $2m$ for $\lambda < \lambda_c$. In this case, the interaction is again repulsive and the phase shift is negative and decreasing.

We use the previous results to study the properties of this QFT at finite temperature by using the phase-shift (or S-matrix) approach, according to which the density of states is proportional to the derivative of the phase shift with respect to the $\sqrt{s}$. For $\lambda > 0$, the contribution of the interaction to the pressure (as well as to other quantities) is negative, in agreement with the repulsive nature of the interaction. On the other hand, for $\lambda_c < \lambda < 0$, the contribution to the pressure is positive, as the attraction suggests.

The case $\lambda < \lambda_c$ requires care: on the one hand, the repulsion causes a negative contribution of the φ-φ interaction to the pressure, but the presence of the bound state implies a positive contribution to the pressure: the net result is a positive contribution. Quite remarkably, the total pressure as function of the coupling constant λ is *continuous* also at $\lambda = \lambda_c$: the jump in pressure generated by the abrupt appearance of the bound state is *exactly* canceled by an analogous jump (but with opposite sign) due to the phase-shift contribution to the pressure. Within this context, we shall extend the S-matrix formalism to include the contribution of eventual bound states. This point represents a formal achievement of our approach and corresponds to a rather intuitive aspect of the problem: the bound state is also an outcome of the two-particle interaction; hence its role should be also described by a (proper) extension of the phase-shift approach below the particle-particle threshold.

In summary, our findings show that the number density of the bound state with mass M_B can be calculated by the "simple" thermal integral

$$n_B = \theta(\lambda_c - \lambda) \int_k \left[e^{-\beta\sqrt{k^2+M_B^2}} - 1 \right]^{-1} \tag{1}$$

for any temperature T (in the previous equation, $\int_k \equiv \int d^3k/(2\pi)^3$). This result is valid also when the mass of the bound state M_B is just below the threshold $2m$ and for temperatures $T \gg 2m - M_B$ (hence, even for temperatures much larger than the binding energy). However, the contribution of the interacting $\varphi\varphi$-system is *not* simply given by the standard contribution to the pressure

$$P_B = -\theta(\lambda_c - \lambda) T \int_k \ln\left[1 - e^{-\beta\sqrt{k^2+M_B^2}} \right], \tag{2}$$

but caution is needed. In general, we shall find that for $\lambda < \lambda_c$ the total interacting contribution to the pressure (including both the bound state and the $\varphi\varphi$-interaction above threshold) can be expressed as

$$\zeta P_B \quad \text{with} \quad 0 < \zeta < 1. \tag{3}$$

For small temperatures, the ratio ζ is close to 1, but for higher temperatures it saturates to a certain finite which is typically about 0.5. Quite interestingly, the existence of this cancellation was discussed in the framework of Quantum Mechanics (QM) in Ref. [21], even if in that case the cancellation was more pronounced (ζ quite small) than the result obtained in our QFT approach.

In conclusion, when a bound state forms in a thermal gas, one should not simply add the corresponding thermal integral as in Eq. (2) to the pressure, since the additional role of the interaction that leads to the very existence of that bound state is not negligible and contributes with an opposite sign.

The paper is organized as follows: in Sec. II we concentrate on the main properties of the system in the vacuum, that include phase shifts, unitarization procedure, and the emergence of a bound state when the attraction is strong enough; then, in Sec. III we present the results at nonzero temperature with special focus on the pressure and the role of the bound state; finally, in Sec. IV we summarize and conclude our paper.

II. VACUUM PHENOMENOLOGY OF SCALAR φ^4-THEORY

A. Scattering phase shifts

In this section we discuss the relatively simple but nontrivial interacting QFT involving a single scalar field φ subject to the Lagrangian

$$\mathcal{L} = \frac{1}{2}(\partial_\mu\varphi)^2 - \frac{1}{2}m^2\varphi^2 - \frac{\lambda}{4!}\varphi^4, \tag{4}$$

where the first two terms describe a free particle with mass m and the last term corresponds to the quartic interaction. The coupling constant λ is dimensionless and the theory is renormalizable [36]. For a detailed analysis of this theory in the context of perturbation theory[1] see Ref. [39]. As we shall comment later on, we will introduce a nonperturbative unitarization procedure on top of Eq. (4), in such a way to make the theory finite, unitary and well defined for each value of the coupling constant λ (even for large ones). This is done at the one-loop resummed level with a suitable subtraction constant.

In the center of mass frame, the differential cross section is given by [36]

[1]The φ^4 QFT could also be trivial, in the sense that the coupling constant vanishes after the renormalization procedure is carried out; see e.g., Refs. [37,38] and refs. therein for the discussion of this issue.

$$\frac{d\sigma}{d\Omega} = \frac{|A(s,t,u)|^2}{64\pi^2 s}, \tag{5}$$

where $A(s,t,u)$ is the scattering amplitude as evaluated through Feynman diagrams, and s, t and u are Mandelstam variables:

$$s = (p_1 + p_2)^2 \geq 4m^2, \tag{6}$$

$$t = (p_1 - p_3)^2 = -\frac{1}{2}(s - 4m^2)(1 - \cos\theta) \leq 0, \tag{7}$$

$$u = (p_2 - p_3)^2 = -\frac{1}{2}(s - 4m^2)(1 + \cos\theta) \leq 0, \tag{8}$$

where p_1, p_2, p_3 and p_4 are four-momenta of the particles (p_1, p_2 ingoing and p_3, p_4 outgoing), and θ is the scattering angle. The sum of these three variables is $s + t + u = 4m^2$. The scattering amplitude can be expressed in terms of partial waves (by keeping s and θ as independent variables) as [40]:

$$A(s,t,u) = A(s,\theta) = \sum_{l=0}^{\infty}(2l+1)A_l(s)P_l(\cos\theta), \tag{9}$$

where $P_l(\xi)$ with $\xi = \cos\theta$ are the Legendre polynomials with

$$\int_{-1}^{+1} d\xi P_l(\xi)P_{l'}(\xi) = \frac{2}{2l+1}\delta_{ll'}. \tag{10}$$

In general, the l-th wave contribution to the amplitude is given by $A_l(s) = \frac{1}{2}\int_{-1}^{+1} d\xi A(s,\theta)P_l(\xi)$.

In the particular case of our Lagrangian of Eq. (4), the tree-level scattering amplitude $A(s,t,u)$ takes the very simple form:

$$iA(s,t,u) = i(-\lambda) \Rightarrow A(s,t,u) = A(s,\theta) = -\lambda. \tag{11}$$

For $\lambda > 0$, one has $A < 0$: the (tree-level) interaction is repulsive. On the other hand for $\lambda < 0$ one has $A > 0$, which corresponds to an attractive interaction. (This case implies that the vacuum $\varphi = 0$ is only metastable, but this shall not affect our discussion.)

At tree level the s-wave amplitude's contribution takes the form:

$$A_0(s) = \frac{1}{2}\int_{-1}^{+1} d\xi A(s,\theta) = A(s,\theta) = -\lambda, \tag{12}$$

while all other waves vanish, $A_{l=1,2,\ldots}(s) = 0$ (this holds true also when unitarizing the theory within the adopted resummation scheme). Further, the total cross section reads

$$\sigma(s) = \frac{1}{2}2\pi\frac{1}{64\pi^2 s}\sum_{l=0}^{\infty}2(2l+1)|A_l(s)|^2 = \frac{1}{32\pi s}|A_0(s)|^2. \tag{13}$$

At threshold:

$$\sigma(s_{th} = 4m^2) = \frac{1}{2}2\pi\frac{1}{64\pi^2 s}2|A_0(s_{th})|^2 = 8\pi|a_0^{\rm SL}|^2, \tag{14}$$

where $a_0^{\rm SL}$ is the s-wave ($l = 0$) scattering length (at tree level) given by:

$$a_0^{\rm SL} = \frac{1}{2}\frac{A_0(s = 4m^2)}{8\pi\sqrt{4m^2}} = \frac{1}{2}\frac{-\lambda}{16\pi m}. \tag{15}$$

The factor $1/2$ in the previous equation refers to identical particles.

Next, we introduce the phase shifts. For identical particles, one has the following general definition of the l-th wave phase shift $\delta_l(s)$:

$$\frac{e^{2i\delta_l(s)} - 1}{2i} = ka_l(s) = \frac{1}{2}\cdot\frac{k}{8\pi\sqrt{s}}A_l(s), \tag{16}$$

where $k = \sqrt{\frac{s}{4} - m^2}$ is the modulus of the three-momentum of one of the ingoing (or outgoing) particles. In the present case, the only nonvanishing phase shift is given by $\delta_0(s)$

$$\frac{e^{2i\delta_0(s)} - 1}{2i} = ka_0(s) = \frac{1}{2}\cdot\frac{k}{8\pi\sqrt{s}}A_0(s), \tag{17}$$

where the "running" length $a_0(s)$ is by construction such that $a_0(s = 4m^2) = a_0^{\rm SL}$. Note, for s just above the threshold we have

$$\frac{e^{2i\delta_0(s)} - 1}{2i} \simeq \delta_0(s) \simeq ka_0^{\rm SL}. \tag{18}$$

In general, the phase shift $\delta_0(s)$ can be calculated as:

$$\delta_0(s) = \frac{1}{2}\arg\left[1 - \frac{1}{16\pi}\sqrt{\frac{4m^2}{s} - 1}A_0(s)\right]. \tag{19}$$

Next, we explore the role of λ for the tree-level scattering. In Fig. 1 we show the behavior of phase shift $\delta_0(s)$ using Eq. (19) for different values of λ. For positive λ values, the function $\delta_0(s)$ is negative and decreases with increasing $\sqrt{s}/m$: the slope of the curve $(\partial\delta_0/\partial\sqrt{s})$ is negative for any arbitrary value of s, which indicates an repulsive interaction. For negative λ values, the opposite behavior is realized, signaling attraction.

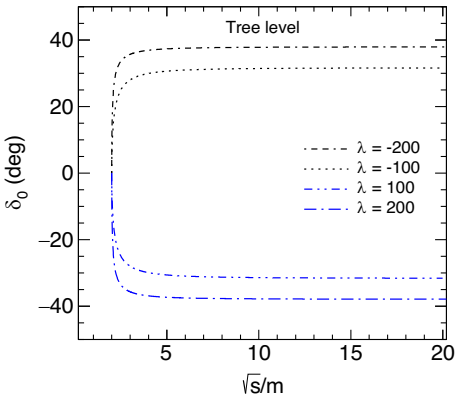

FIG. 1. Behavior of the phase shift at the tree level for different values of λ.

The asymptotic values $\delta_0(s \to \infty)$ do not tend to a multiple of π, since the theory at first order in λ is only unitary at that order. As a consequence, we can trust the results only when $\delta_0(s)$ is sufficiently small. As a related side remark, the expression $\delta_0(s) = \frac{1}{2}\arcsin\left[\frac{k}{8\pi\sqrt{s}}A_0(s)\right]$ [which in principle follows from Eq. (17)] is also valid only when the amplitude is sufficiently small. This drawback is also due to the lack of unitarity.

All these aspects show that the unitarization is necessary, as we show in detail in the next subsection.

B. Unitarization

Here, we introduce the two-particle loop of the field φ, that we denote as $\Sigma(s)$. We start from the requirement about its imaginary part above threshold (because of the optical theorem):

$$I(s) = \mathrm{Im}\Sigma(s) = \frac{1}{2}\frac{\sqrt{\frac{s}{4} - m^2}}{8\pi\sqrt{s}} \quad \text{for } \sqrt{s} > 2m. \tag{20}$$

We shall put here no cutof; hence the above equation is considered valid up to arbitrary values of the variable s [note, in each realistic QFT the quantity $\mathrm{Im}\Sigma(s)$ should decrease for s large enough, e.g., above the GUT or the Planck scale; nevertheless, from a mathematical point of view, we can get a fully consistent treatment for any value of s]. The loop function $\Sigma(s)$ for complex values of the variable s reads

$$\Sigma(s) = \frac{1}{\pi}\int_{4m^2}^{\infty} ds' \frac{I(s')}{s' - s - i\epsilon} - C, \tag{21}$$

where the subtraction C guarantees convergence. Here, we make the choice $\Sigma(s \to 0) = 0$; hence

$$C = \frac{1}{\pi}\int_{4m^2}^{\infty} ds' \frac{I(s')}{s'}. \tag{22}$$

This choice turns out to be very convenient for our purposes. Explicitly, the loop reads (we keep track of the arbitrary small ϵ since this will be important later on):

$$\Sigma(s) = \frac{1}{2}\frac{1}{16\pi}\left(-\frac{1}{\pi}\sqrt{1 - \frac{4m^2}{s + i\epsilon}}\ln\frac{\sqrt{1 - \frac{4m^2}{s+i\epsilon}} + 1}{\sqrt{1 - \frac{4m^2}{s+i\epsilon}} - 1}\right) + \frac{1}{16\pi^2}. \tag{23}$$

(For details on the $\varphi\varphi$ loops, see Ref. [41] and references therein.) For s being real we get

$$\mathrm{Im}\Sigma(s) = \begin{cases} \frac{1}{2}\frac{\sqrt{\frac{s}{4} - m^2}}{8\pi\sqrt{s}} & \text{for } s > (2m)^2 \\ \varepsilon & \text{for } s < (2m)^2, \end{cases} \tag{24}$$

where $\varepsilon \propto \epsilon$ is an infinitesimal positive quantity. Note. Eq. (20) is fulfilled, as it should. Moreover, for s real and larger than $4m^2$, the real part of the loop is given by the principal part (P) of the following integral:

$$\mathrm{Re}\Sigma(s) = \frac{s}{\pi}P\int_{s_{th}}^{\infty} \frac{I(s')}{(s' - s)s'}. \tag{25}$$

The functions $\mathrm{Im}\Sigma(s)$ and $\mathrm{Re}\Sigma(s)$ (for real values of s) are presented in Fig. 2. The real part rises below threshold, has a cusp at it, then decreases monotonically and becomes negative for $\sqrt{s}/m$ large enough. The imaginary part is zero (infinitesimally small) below threshold, then it rises above it and saturates to the value $1/(32\pi)$ for large $\sqrt{s}/m$. Note, its right-hand-side derivative at threshold is infinite.

The loop function allows to calculate the unitarized amplitudes in the k-channel as:

$$A_k^U(s) = [A_k^{-1}(s) - \Sigma(s)]^{-1}. \tag{26}$$

All unitarized amplitudes (and consequently phase shifts) with $l = 1, 2, \ldots$ vanish also at the unitarized level. The unitarized s-wave amplitude and phase shift are nonzero and take the form:

$$A_0^U(s) = [A_0^{-1}(s) - \Sigma(s)]^{-1} = \frac{-\lambda}{1 + \lambda\Sigma(s)}, \tag{27}$$

$$\frac{e^{2i\delta_0^U(s)} - 1}{2i} = \frac{1}{2}\cdot\frac{k}{8\pi\sqrt{s}}A_0^U(s). \tag{28}$$

Hence

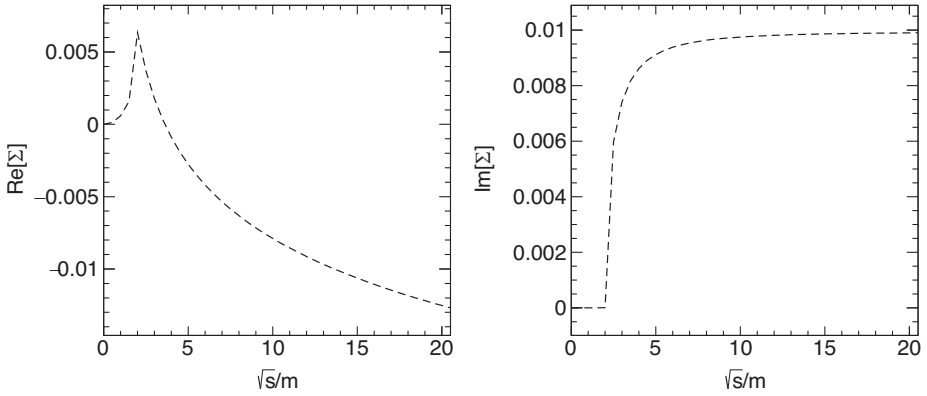

FIG. 2. Real and imaginary parts of loop function for real $\sqrt{s}/m$.

$$\delta_0^U(s) = \frac{1}{2}\arg\left[1 - \frac{1}{8\pi}\sqrt{\frac{m^2}{s} - \frac{1}{4}}A_0^U(s)\right]. \tag{29}$$

The scattering length is changed by the unitarization:

$$a_0^{U,\mathrm{SL}} = \frac{1}{2}\frac{A_0^U(s=4m^2)}{8\pi\sqrt{4m^2}} = \frac{1}{2}\frac{1}{16\pi m}\frac{-\lambda}{1+\lambda\Sigma(4m^2)}. \tag{30}$$

Within the used unitarization

$$\Sigma(s=4m^2) = \frac{1}{16\pi^2}; \tag{31}$$

hence it follows that

$$a_0^{U,\mathrm{SL}} = \frac{1}{2}\frac{1}{16\pi m}\frac{-\lambda}{1+\frac{\lambda}{16\pi^2}}. \tag{32}$$

It is then clear that $a_0^{U,\mathrm{SL}} < 0$ for $\lambda > 0$ (repulsion), and that $a_0^{U,\mathrm{SL}} > 0$ for $\lambda \in (\lambda_c = -16\pi^2, 0)$ (attraction). However, $a_0^{U,\mathrm{SL}} < 0$ for $\lambda < \lambda_c$, in agreement with the fact that repulsion sets in again. This is due to the fact that for $\lambda < \lambda_c$ a bound state below threshold emerges, as we shall show in the next subsection.

Finally one can calculate $\delta_0^U(s)$ by using the equivalent expressions

$$\delta_0^U(s) = \frac{1}{2}\arcsin\left[\frac{k}{8\pi\sqrt{s}}\mathrm{Re}[A_0^U(s)]\right], \tag{33}$$

$$\delta_0^U(s) = \frac{1}{2}\arccos\left[1 - \frac{k}{8\pi\sqrt{s}}\mathrm{Im}[A_0^U(s)]\right]. \tag{34}$$

Once the unitarization procedure is employed, the expressions (33), (34), and (28) give rise to the same result for the phase shift. This is also a useful check of the correctness of our approach.

C. Bound state

If λ is negative the two scalar particles attract each other. A natural question is under which condition a bound state emerges. Such a bound state, denoted as B, with mass M_B, should fulfill the equation [for $s \in (0, 4m^2)$]

$$A_0^U(s)^{-1} = [-\lambda^{-1} - \Sigma(s = M_B^2)] = 0. \tag{35}$$

Since $\Sigma(s)$ is real for $s < 4m^2$ and has a maximum at threshold with $\Sigma(s=4m^2) = \frac{1}{16\pi^2}$ [see Eq. (23)], it turns out that a bound state is present if

$$\lambda \le \lambda_c = -16\pi^2. \tag{36}$$

The mass M_B as a function of λ, plotted in Fig. 3, fulfills the conditions:

$$M_B(\lambda = \lambda_c) = 2m, \tag{37}$$

$$M_B(\lambda \to -\infty) = 0. \tag{38}$$

This result also shows the convenience of the employed subtraction scheme: when the attraction is infinitely strong, the bound state becomes massless. This choice avoids

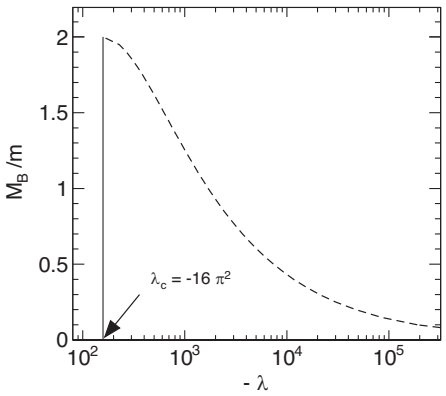

FIG. 3. Mass of the bound state M_B as function of $-\lambda$.

also the emergence of an additional energy scale into the problem.

Of course, one could perform the study also for different subtraction choices: if e.g., $\Sigma(0) > 0$ the mass M_B tends to a finite value for an infinite negative coupling; if, instead, $\Sigma(0) < 0$ a tachyonic mode (instability) appears for a negative coupling whose modulus is large enough. Alternatively, one could use a finite cutoff function, but this choice is linked to a nonlocal Lagrangian [42–44]. Yet, all these possibilities imply that a new energy scale enters into the problem. While this might be possible, that would introduce an unnecessary complication and would also spoil the fact that only the mass m entering in Eq. (4) is the unique energy scale of the system.

In conclusion, the quartic theory of Eq. (4) is fully defined only once its unitarization is settled. The unitarized version of the model together with the employed subtraction constant chosen in this work assures that the model under study is well defined for any λ (positive and negative) and is therefore very well suited for the study that we aim to do, namely the role of the bound state in a thermal bath.

D. Behavior of the unitarized phase shift

In order to discuss unitarized phase shift, an important note on the adopted convention is in order. We impose that the phase shift vanishes at threshold:

$$\delta_0^U(s = 4m^2) = 0, \tag{39}$$

regardless of the existence of the bound state below threshold or not. In this way, the comparison between different curves is better visible. We recall that often a different convention is used, according to which the phase space at threshold equals $n_{BS}\pi$, where n_{BS} is the number of bound states below threshold [45]. Of course, the choice of the convention has no impact on the physics. For instance, the Levinson theorem [46,47] relates the number of poles below threshold to the difference of the phase shift at infinity and at threshold:

$$n_{\text{poles-below-threshold}} = \frac{1}{\pi}(\delta_0^U(s \to \infty^2) - \delta_0^U(s = 4m^2)). \tag{40}$$

This quantity is clearly independent on the choice of an overall constant. In some cases, the number of poles below threshold equals the number of bound states, but care is needed, since some unphysical poles may also exist; see below.

Similarly, the finite temperature properties studied in the next section depend on the derivative $d\delta_0^U(s)/ds$, which is also independent on the convention regarding $\delta_0^U(s = 4m^2)$. We shall also elaborate more on the behavior of $\delta_0^U(s)$ in Sec. III.3.

Let us now present the behavior of the unitarized phase shift $\delta_0^U(s)$ in Fig. 4. Only for small λ, the behavior of $\delta_0(s)$

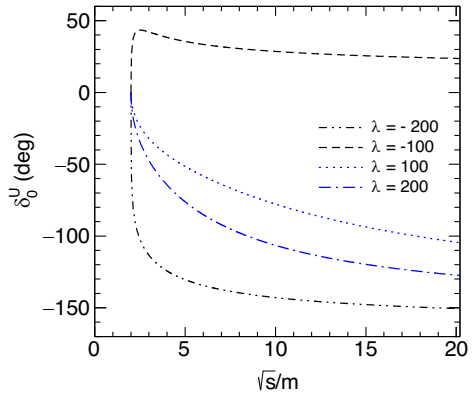

FIG. 4. Behavior of the unitarized phase shift δ_0^U as function of $\sqrt{s}/m$ for different values of λ.

is similar to that of Fig. 1. Yet, also in the unitarized case, for $\lambda > 0$ the phase shift and its derivative are always negative. Moreover, the asymptotic value

$$\delta_0^U(s \to \infty) = -\pi \quad \text{for } \lambda > 0 \tag{41}$$

is realized. In addition, the point at which $\delta_0^U(s = s_1) = -\pi/2$ is obtained for

$$-\lambda^{-1} - \text{Re}\Sigma(s_1) = 0, \tag{42}$$

where the amplitude becomes purely imaginary with

$$\frac{e^{2i\delta_0(s_1)} - 1}{2i} = i. \tag{43}$$

The point s_1 is present for each positive value of λ since $\text{Re}\Sigma(s_1)$ is unbounded from below. According to the Levinson theorem [46,47], Eq. (41) implies that a pole below threshold exists. Indeed, for $\lambda > 0$ such a pole of the amplitude is present for a negative value of s that fulfills the very same Eq. (35), but of course this pole does not correspond to a physical bound state.

Next, for λ negative but belonging to the range $(\lambda_c = -16\pi^2, 0)$, the phase shift is positive, it rises for small values of $\sqrt{s}/m$, it reaches a maximum, and than it bends over approaching zero for large values of s:

$$\delta_0^U(s \to \infty) = 0 \quad \text{for } \lambda \in (\lambda_c, 0). \tag{44}$$

This is also in agreement with the Levinson's theorem, since no pole below threshold appears.

Finally, for $\lambda < \lambda_c$ the phase $\delta_0^U(s)$ is negative and approaches $-\pi$:

$$\delta_0^U(s \to \infty) = -\pi \quad \text{for } \lambda < \lambda_c, \tag{45}$$

in accordance with Levinson's theorem, since a pole for $s = M_B^2$ exists. Also in this case, there is a certain value $s = s_1$ at which the phase is $-\pi/2$.

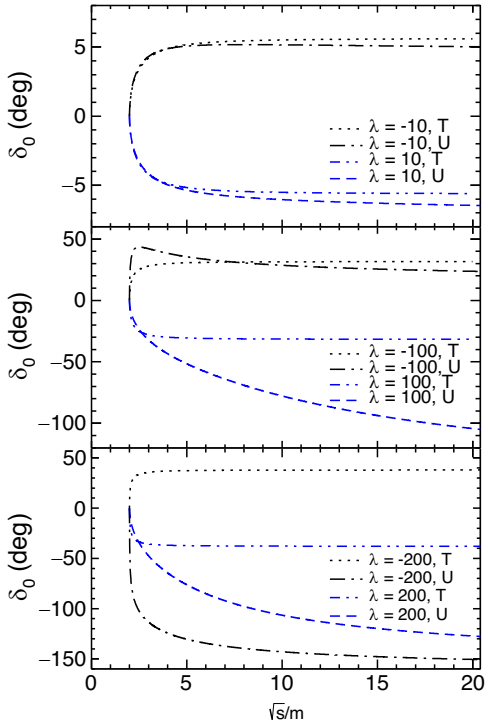

FIG. 5. Comparison of tree-level (T) and unitarized (U) phase shifts as function of $\sqrt{s}/m$ for different values of λ. As we discuss in the text, the phase shift is chosen to vanish at threshold $[\delta_0^U(s=4m^2)=0]$, independently of the value of λ. In this way it is easy to compare the behavior of the phase shift for different values of λ, even when a bound state emerges. This choice does not affect the physics.

In Fig. 5 we compare the tree-level (T) and the unitarized (U) phase shifts. The top panel shows the results when λ is small (± 10). The qualitative behavior of the phase shifts for both cases is similar for all $\sqrt{s}/m$ shown in the figure. When $\sqrt{s}/m$ is small (<4), the tree-level and unitarized results are very close to each other, then a discrepancy is appreciable at larger values of $\sqrt{s}/m$. In the middle panel we show a similar comparison for $\lambda = \pm 100$. In this case the unitarized phase shifts differ significantly from the tree-level ones. For $\lambda = -100$, the unitarized phase shift first increases sharply for increasing $\sqrt{s}/m$, reaches a maximum, and then starts decreasing. The magnitude of the unitarized phase shift is larger than that at tree level at low $\sqrt{s}/m$, but becomes smaller at large $\sqrt{s}/m$. For $\lambda = +100$ both the tree-level and the unitarized phase shift decrease for increasing $\sqrt{s}/m$. However, the decrease is much steeper for the unitarized phase shift. The bottom panel of Fig. 5 shows the choice $\lambda = \pm 200$. For $\lambda = 200$ the comparison of the tree-level and unitarized phase shift is similar to that of $\lambda = 100$. However, the behavior of unitarized phase shift for $\lambda = -200$ is completely different from the tree-level one. While tree-level phase shift is positive, the unitarized phase shift is negative because $\lambda < \lambda_c$. Correspondingly, in this case the bound state that dominates the near-threshold phenomenology is built.

III. THERMODYNAMICAL PROPERTIES OF THE THEORY

We now consider the thermodynamics (TD) of the system at nonzero temperature. We first discuss the pressure of the system by using the phase-shift approach at tree level, in which no bound state is present, and then at the unitarized one-loop level. Within the latter scheme, we study the contribution to the TD of an emerging bound state when the attraction is large enough to form it ($\lambda \leq \lambda_c$).

A. Pressure without the bound state: Tree-level results

The noninteracting part of the pressure for a gas of particles with mass m reads:

$$P_{\varphi,\text{free}} = -T \int_k \ln\left[1 - e^{-\beta\sqrt{k^2+m^2}}\right]. \tag{46}$$

In the S-matrix formalism [48–56], the interacting part of the pressure is related to the derivative of the phase shift with respect to the energy by the following relation:

$$P_{\varphi\varphi\text{-int}} = -T \int_{2m}^{\infty} dx \frac{2l+1}{\pi} \sum_{l=0}^{\infty} \frac{d\delta_l(s=x^2)}{dx} \times \int_k \ln\left[1 - e^{-\beta\sqrt{k^2+x^2}}\right], \tag{47}$$

where $x = \sqrt{s}$. In our specific case, only the s-wave contribution is nonzero:

$$P_{\varphi\varphi\text{-int}} = -T \int_{2m}^{\infty} dx \frac{1}{\pi} \frac{d\delta_0(s=x^2)}{dx} \int_k \ln\left[1 - e^{-\beta\sqrt{k^2+x^2}}\right]. \tag{48}$$

Then, the total tree-level pressure (obviously in the absence of a bound state, since at tree level it cannot be generated) is given by

$$P_{\text{tot}} = P_{\varphi,\text{free}} + P_{\varphi\varphi\text{-int}} \quad \text{(at tree level)}. \tag{49}$$

The previous equations show that we can evaluate the pressure at $T > 0$ by using solely the phase shift evaluated in the vacuum. Of course, all other relevant thermodynamic quantities of the thermal system (such as energy and entropy densities, etc.) can be determined once the pressure is known.

The temperature dependence of the corresponding pressure $(P_{\varphi,\text{free}} + P_{\varphi\varphi\text{-int}})/T^4$ is shown in Fig. 6. The $\lambda = 0$ line corresponds to the pressure of a free gas $P_{\varphi,\text{free}}/T^4$ that for large T/m saturates towards the massless limit

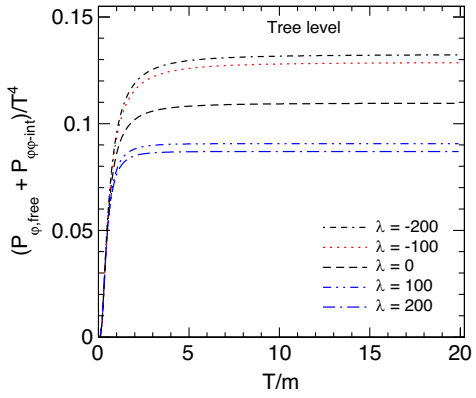

FIG. 6. Tree-level plots of the normalized pressure as function of T/m for different values of λ.

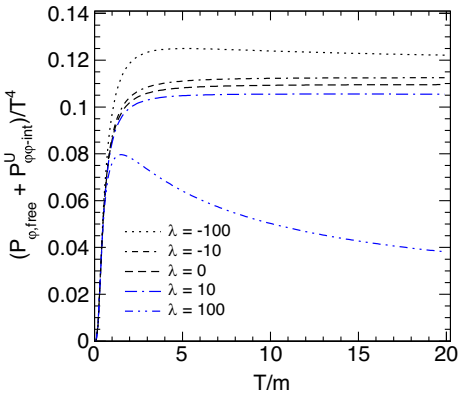

FIG. 8. Temperature dependence of the normalized pressure in the unitarized case for $\lambda = \pm 10$ and for $\lambda = \pm 100$.

($P_{\varphi,\text{free}}/T^4_{m=0} = \pi^2/90$). For positive (negative) λ, the tree-level repulsive (attractive) interaction implies that the pressure is smaller (larger) than the noninteracting case, but never exceeds 0.5. As we shall see, the unitarization enhances the contribution of the interaction.

Next, in Fig. 7 we study $P_{\varphi\varphi\text{-int}}/T^4$ and $P_{\varphi\varphi\text{-int}}/P_{\varphi,\text{free}}$ as function of λ for four different m/T ratios 2, 1, 0.5 and 0.2. One can see that near $\lambda = 0$, $P_{\varphi\varphi\text{-int}}/T^4$ changes rapidly with λ, but then saturates at large values of λ. In the right panel, one can see that all the curves of the function $P_{\varphi\varphi\text{-int}}/P_{\varphi,\text{free}}$ cross the origin at $\lambda = 0$, which is expected since there is no interaction at $\lambda = 0$. Further, it can be seen that the effect of the interaction is larger both for large λ and/or low m/T.

B. Pressure without the bound state: Unitarized results

When including the unitarization procedure explained in Sec. II B, the interaction contribution to the pressure is obtained by using the unitarized phase shift into the S-matrix formalism:

$$P^U_{\varphi\varphi\text{-int}} = -T\int_{2m}^{\infty} dx \frac{1}{\pi}\frac{d\delta_0^U(s=x^2)}{dx}\int_k \ln\left[1 - e^{-\beta\sqrt{k^2+x^2}}\right]. \tag{50}$$

Then, the total pressure (in the absence of a bound state) is given by

$$P^U_{\text{tot}} = P_{\varphi,\text{free}} + P^U_{\varphi\varphi\text{-int}} \quad (\text{unitarized, for } \lambda > \lambda_c). \tag{51}$$

Figure 8 shows the temperature dependence of pressure in the unitarized case. [Note, no bound state contribution is present here since all the considered values of the coupling λ are larger than λ_c.] For small λ (± 10), the normalized pressure saturates at large T/m.

Yet, for $\lambda = \pm 100$ the normalized pressure as a function of the temperature is quite different from the noninteracting case, since it reaches a maximum for a finite value of the temperature. In general, this figure shows that for large values of λ and for large temperatures, the unitarized result is sizably different from the tree-level result reported in Fig. 6.

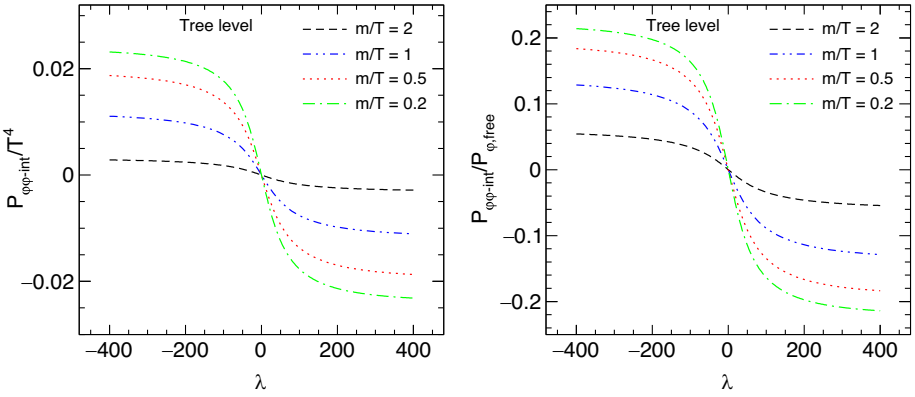

FIG. 7. The left panel shows the normalized pressure at tree level as function of λ for different temperatures. The right panel shows the ratio of the interacting pressure over the pressure of a free gas as function of λ for different temperatures.

C. The general case: Inclusion of the bound state, formal aspects, and numerical results

The crucial question of the present work is how to include the effect of the emergent bound state B in the thermodynamics. The easiest way is to add to the pressure of the system the pressure of mass M_B as:

$$P_B = -\theta(\lambda_c - \lambda) T \int_k \ln\left[1 - e^{-\beta\sqrt{k^2+M_B^2}}\right], \quad (52)$$

where the theta function takes into account that for $\lambda > \lambda_c$ there is no bound state B. Of course, M_B is itself also a function of λ, see Eq. (35) and Fig. 3.

Within this context, the full (unitarized) pressure looks like

$$P^U_{\rm tot} = P_B + P_{\varphi,\rm free} + P^U_{\varphi\varphi\text{-int}} \ \ (\text{unitarized, for any } \lambda). \quad (53)$$

Quite remarkably, $P^U_{\rm tot}$ turns out to be a continuous function of λ, even if P_B is not continuous at $\lambda = \lambda_c$ since it jumps abruptly from 0 to a certain finite value. Yet, the quantity $P^U_{\varphi\varphi\text{-int}}$ is also not continuous in such a way to compensate the previous jump; see below.

The issue is if the inclusion of P_B as in Eq. (52) is correct. To study this point, we discuss how the contribution of the bound state can be formally included into the phase-shift analysis, showing that the simple prescription of adding one additional state to the thermodynamics is correct and the result is independent on the residuum of the pole of the bound state.

In order to show these features, let us first modify Eq. (28) by extending its validity also below the threshold. To this end we consider

$$\frac{e^{2i\delta_0^U(s)} - 1}{2i} = \mathrm{Im}\Sigma(s) \cdot A_0^U(s), \quad (54)$$

where $\mathrm{Im}\Sigma(s)$ is given by Eq. (24). Clearly, above threshold nothing changes. On the other hand, below threshold we get the following expression:

$$\frac{e^{2i\delta_0^U(s)} - 1}{2i} = \varepsilon A_0^U(s) = \frac{\varepsilon}{A_0^{-1}(s) - \Sigma(s)}. \quad (55)$$

Note, if ε is set strictly to zero, we get obviously zero. If there is no pole below threshold, δ_0^U is an infinitesimally small number, that can be set to zero and has no effect in the description of the system.

Next, let us assume that a bound state below threshold appears: $A_0^{-1}(s) - \Sigma(s) = 0$ for $s = M_B^2 \in (0, 4m^2)$. In this case, we have (below threshold):

$$\frac{e^{2i\delta_0^U(s)} - 1}{2i} = \frac{\varepsilon}{-Z^{-1}(s - M_B^2) + i\varepsilon} \quad (\text{for } 0 < s < 4m^2), \quad (56)$$

where

$$Z = \frac{1}{\Sigma'(s = M_B^2)}. \quad (57)$$

Using the expression for the phase shift of Eq. (34) we find:

$$\delta_0^U(s) = \frac{1}{2}\arccos\left[1 - \frac{2\varepsilon^2}{[Z^{-1}(s - M_B^2)]^2 + \varepsilon^2}\right] \quad (\text{for } 0 < s < 4m^2). \quad (58)$$

For $0 < s < M_B^2$ the argument of the arccos is 1 (for an arbitrary small ε), then unitarized phase shift $\delta_0^{\rm U} = n\pi$, where n is an integer. We recall that it in this work we require that $\delta_0^U(s)$ vanishes at threshold:

$$\delta_0^U(s = 4m^2) = 0. \quad (59)$$

By assuming that there is a single pole below threshold, for $s < M_B^2$ it is useful to impose that $n = -1$:

$$\delta_0^U(0 < s < M_B) = -\pi \quad \text{for } 0 < s < M_B^2. \quad (60)$$

Next, we notice that for $s = M_B^2$, the argument equals to $1 - \frac{2\varepsilon^2}{\varepsilon^2} = -1$, therefore $\delta_0^U = \frac{n}{2}\pi$ for this particular choice of s.

The function $\delta_0^U(s = x^2)$ must be (for a finite ε, even if arbitrarily small) a continuous and differentiable function. Hence, it follows that

$$\delta_0^U(s = M_B^2) = -\frac{\pi}{2}. \quad (61)$$

Moreover, for any value of $M_B^2 < s < 4m^2$ we have

$$\delta_0^U(M_B^2 < s < 4m^2) = 0. \quad (62)$$

We may then conclude that for $s \in (0, 4m^2)$, alias for $x \in (0, 2m)$, the phase shift takes the form:

$$\delta_0^U(x = \sqrt{s}) = -\pi + \pi\theta(x - M_B). \quad (63)$$

In this way we obtain the desired result:

$$\frac{1}{\pi}\frac{d\delta_0^U(x)}{dx} = \delta(x - M_B). \quad (64)$$

Quite interestingly, this result is independent on the residue of the pole Z. The bound state counts always as 1, showing that the corresponding density of states is given by

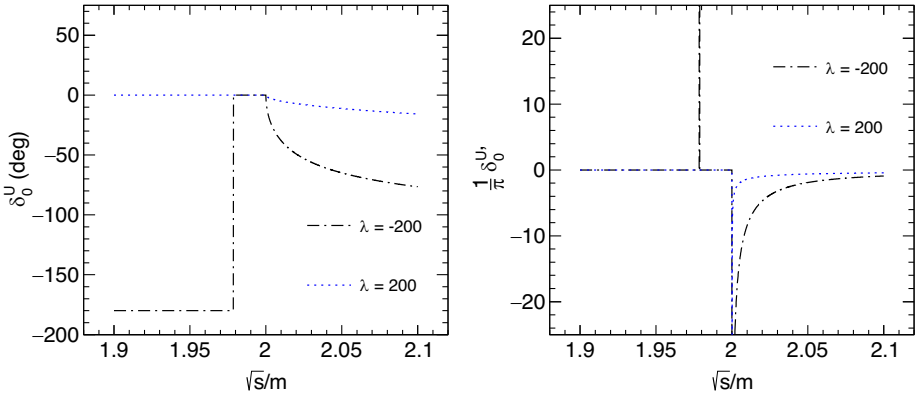

FIG. 9. Left panel shows the energy dependence of the unitarized phase shift for $\lambda = \pm 200$. Right panel shows the derivative of the corresponding phase shifts.

$$n_B = \theta(\lambda_c - \lambda) \int_k \left[e^{-\beta\sqrt{k^2+M_B^2}} - 1 \right]^{-1}, \tag{65}$$

in agreement with thermal models.

In order to understand better the behavior of the phase shift, we show in the left panel of Fig. 9 the behavior of the unitarized phase shift below threshold for two different λ values, one below and another above the critical value. For $\lambda = 200 > \lambda_c$, the phase shift is simply zero below the threshold and decreases with the increase of $\sqrt{s}/m$, whereas, for $\lambda = -200 < \lambda_c$, the phase shift is $-\pi$ (according to our convention) below the mass of the bound state ($M_B/m \sim 1.98$). The phase shift jumps to zero for $\sqrt{s} = M_B$ and remains zero up to the threshold. This jump of phase shift is due to the formation of the bound state. Above threshold the phase shift decreases with the increase of $\sqrt{s}/m$.

The right panel of Fig. 9 shows the energy dependence of the derivative of the phase shift. For $\lambda = 200$, the derivative of the phase shift is zero below threshold. Above threshold this quantity is negative and its magnitude increases with the increase of $\sqrt{s}/m$. For $\lambda = -200$, there is a delta function at $\sqrt{s} = M_B$, which is responsible for the inclusion of the bound state in the phase-shift formalism. Indeed, as shown in Eq. (50), the pressure depends on the derivative of the phase shift, hence the functions depicted in the right panel of Fig. 9 represent the two-particle energy weight.

One can also understand from the plots in Fig. 9 that, using the more common convention according to which the phase shift equals π at threshold when a bound state is present, would amount to consider $\delta_0^U(s) + \pi$ for $\lambda = -200$ in the left panel, while the right panel would remain unchanged. This result shows that the choice of the phase-shift value at threshold does not affect the thermodynamics (as well as any other physical property), as it should.

Finally, we turn to the thermodynamics of the system. The pressure contributions from the bound state and from the interaction can be described by the following expression:

$$\begin{aligned} P_{\varphi\varphi\text{-int-tot}} &= P^U_{\varphi\varphi\text{-int}} + P_B \\ &= -T \int_0^\infty dx \frac{1}{\pi} \frac{d\delta_0^U(s = x^2)}{dx} \\ &\quad \times \int_k \ln\left[1 - e^{-\beta\sqrt{k^2+x^2}}\right], \end{aligned} \tag{66}$$

where the lower bound of the integral is now set to zero. If the bound state is present, it is *automatically* taken into account (independently on the binding energy).

Next, we discuss the numerical result in presence of a bound state. As we have already mentioned, the formation of bound state is possible when λ is less than the critical value $\lambda_c = -16\pi^2$.

Figure 10 shows the temperature dependence of the normalized total pressure for $\lambda = \pm 200$. For the value $\lambda = -200$ (which is less than λ_c) the bound state is present and, as expected, the total normalized pressure is larger than that of noninteracting particle. For the value $\lambda = 200$ the total pressure is strongly reduced. Yet, in general, the qualitative behavior of the curves for $\lambda = \pm 200$ is quite similar to those for $\lambda = \pm 100$ depicted in Fig. 8.

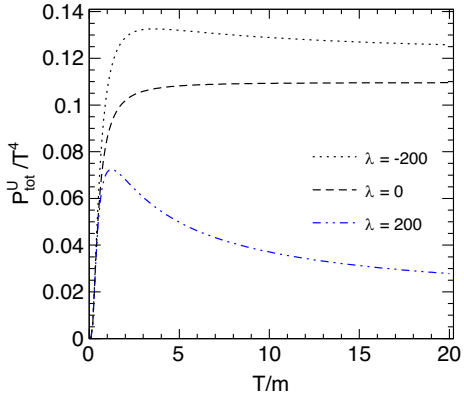

FIG. 10. Temperature dependence of the normalized pressure in the unitarized case for $\lambda = \pm 200$.

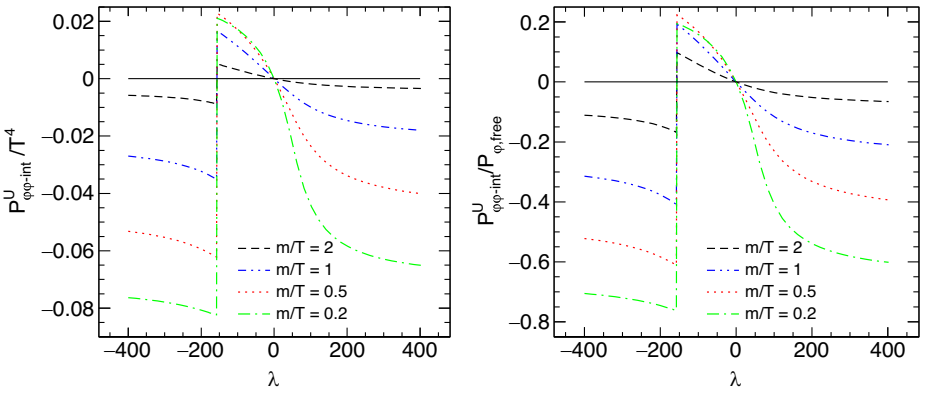

FIG. 11. The left panel shows the behavior of the interacting part of the normalized pressure with λ. The right panel shows the λ-dependence of the interacting part of the pressure relative to that of a free gas of particles with mass m.

The left panel of Fig. 11 shows the variation of the interacting part of normalized pressure with λ (excluding the contribution of the bound state) using the unitarized phase shift. Unlike the tree-level result (left panel of Fig. 7), the interacting pressure in the present case is discontinuous at $\lambda = \lambda_c$. In fact, for $\lambda < \lambda_c$, the interacting part of the pressure becomes negative as a consequence of the bound state. The right panel of Fig. 11 shows the λ-dependence of interacting part of the pressure relative to that of a free gas. It shows that for λ of the order (or larger) of 200, the interacting part of the pressure is definitely sizable.

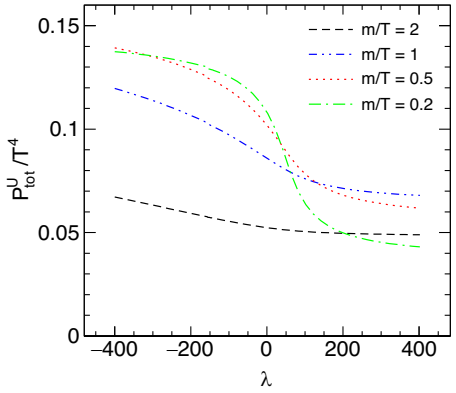

FIG. 12. Total pressure as function of λ for different values of the temperature.

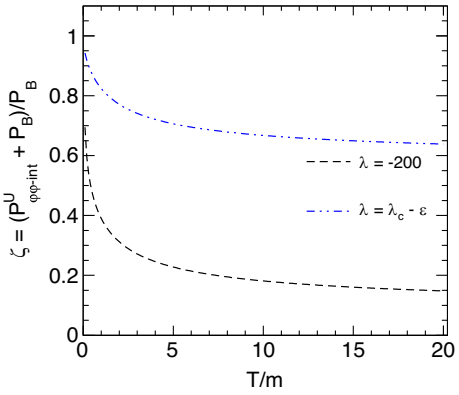

FIG. 13. Variation of ζ with T/m for two different λ below the critical value.

Figure 12 shows the behavior of the normalized total pressure as function of λ. Here, both the contribution of the bound state and of the $\varphi\varphi$ interaction above threshold are included. Quite remarkably, the total pressure is a continuous function also at $\lambda = \lambda_c$: the discontinuity of the interacting part of the pressure shown in the left panel of Fig. 12 is compensated by an analogous (but with opposite sign) jump of the bound state pressure.

Finally, in Fig. 13 we show the variation of ζ

$$\zeta(T,\lambda) = \frac{P^U_{\varphi\varphi\text{-int}} + P_B}{P_B} \tag{67}$$

as function of T/m for two different values of λ for which the bound states form: one just below the critical value, λ_c, and a value sizably below it, $\lambda = -200$. This ratio approaches unity when $P^U_{\varphi\varphi\text{-int}}$ is zero. When λ is just below λ_c, this ratio is close to unity only at low T/m; it then decreases with the increase of T/m and eventually saturates around 0.6 at higher T/m, so even at high temperature T/m this fraction is not negligible. Although the magnitude of ζ is smaller, the trend is similar in case of $\lambda = -200$ as well.

The results suggest that for a bound state created close to threshold (thus λ smaller but close to λ_c), the bound state is indeed important, and the negative contribution to the pressure generated by the particle-particle interaction does not overcome the positive contribution of the bound state. In that case, one should better include the contribution of the bound state to the pressure, but eventually one should take into account that its quantitative role is diminished by the interaction above threshold.

IV. SUMMARY

In this work we have investigated bound states in a thermal gas in the context of QFT. To do this, a QFT involving a single scalar particle with mass m subject to a φ^4-interaction has been used. Besides the tree-level results, we have employed a unitarized one-loop resummed approach for which the theory is finite and well defined for each value of the coupling constant λ and for which no new energy scale appears in the theory. Moreover, for $\lambda < \lambda_c$ a bound state forms.

The phase shift of the s-wave scattering has been calculated using the partial wave decomposition of two body scattering and has been used to calculate the properties of the system at finite temperature through the phase-shift (or S-matrix) approach, according to which the density of states is proportional to the derivative of the phase shift with respect to the running energy $\sqrt{s}$.

For $\lambda > 0$, the contribution of the interaction to the pressure is always negative, in agreement with the repulsive nature of the interaction. On the other hand, for $\lambda_c < \lambda < 0$, the contribution to the pressure is positive indicating an attractive interaction. Below λ_c the interacting part of the pressure due to two-body scattering switches sign: it becomes negative due to the bound state below threshold. Yet, the additional contribution of a gas of bound states makes the total pressure continuous with respect to the coupling λ.

In summary, the contribution of the bound state to the pressure as usually calculated in thermal models is actually diminished by the contribution of the interaction among the fields, but it is not fully canceled. Especially in the case in which the mass of the bound state is close to $2m$ (the nonrelativistic case, realized for λ smaller but close to λ_c), the bound state has a sizable contribution to the pressure (and thus to the thermodynamics). This contribution needs to be eventually corrected by an appropriate multiplicative parameter ζ due to the role of the particle-particle interaction above threshold. Yet, it turns out to be larger than 0.6. We conclude that bound states (such as nuclei or other molecular states in QCD) should not be neglected in thermal models, even if their concrete pressure contribution can be somewhat smaller than the value of the corresponding thermal integrals. Moreover, the multiplicity of such bounds states can be calculated by the usual expression for the thermal number density, regardless of the temperature at which the gas is considered, even if it is much larger than the binding energy of the bound state.

In the future, one can repeat the present analysis by using other types of QFT, eventually by including fermionic fields. We expect that the general picture should be quite stable and independent on the precise adopted model, but it would be important to directly verify this statement. Moreover, one could also calculate the parameter ζ in some concrete examples, such as for the deuteron or for the predominantly molecularlike state $X(3872)$.

ACKNOWLEDGMENTS

The authors acknowledge useful discussions with W. Broniowski and S. Mrówczynski. S. S. is supported by the Polish National Agency for Academic Exchange through Ulam Scholarship with Agreement No. PPN/ULM/2019/1/00093/U/00001. F. G. acknowledges support from the Polish National Science Centre NCN through the OPUS Project No. 2019/33/B/ST2/00613.

[1] V. T. Cocconi, T. Fazzini, G. Fidecaro, M. Legros, N. H. Lipman, and A. W. Merrison, Mass Analysis of the Secondary Particles Produced by the 25-Gev Proton Beam of the Cern Proton Synchrotron, Phys. Rev. Lett. **5**, 19 (1960).

[2] B. I. Abelev *et al.* (STAR Collaboration), Observation of an antimatter hypernucleus, Science **328**, 58 (2010).

[3] H. Agakishiev *et al.* (STAR Collaboration), Observation of the antimatter helium-4 nucleus, Nature (London) **473**, 353 (2011); Erratum, Nature (London) **475**, 412 (2011).

[4] J. Adam *et al.* (ALICE Collaboration), Production of light nuclei and antinuclei in pp and Pb-Pb collisions at energies available at the CERN large hadron collider, Phys. Rev. C **93**, 024917 (2016).

[5] J. Adam *et al.* (STAR Collaboration), Measurement of the mass difference and the binding energy of the hypertriton and antihypertriton, Nat. Phys. **16**, 409 (2020).

[6] S. Acharya *et al.* (ALICE Collaboration), Production of (anti-)^{3}He and (anti-) ^{3}H in p-Pb collisions at $\sqrt{s_{\mathrm{NN}}} =$ 5.02 TeV, Phys. Rev. C **101**, 044906 (2020).

[7] S. Acharya *et al.* (ALICE Collaboration), (Anti-)deuteron production in pp collisions at $\sqrt{s} = 13$ TeV, Eur. Phys. J. C **80**, 889 (2020).

[8] A. Esposito, A. L. Guerrieri, F. Piccinini, A. Pilloni, and A. D. Polosa, Four-quark hadrons: An updated review, Int. J. Mod. Phys. A **30**, 1530002 (2015).

[9] R. Aaij *et al.* (LHCb Collaboration), Observation of a Narrow Pentaquark State, $P_c(4312)^+$, and of Two-Peak Structure of the $P_c(4450)^+$, Phys. Rev. Lett. **122**, 222001 (2019).

[10] K.-J. Sun, L.-W. Chen, C. M. Ko, and Z. Xu, Probing QCD critical fluctuations from light nuclei production in relativistic heavy-ion collisions, Phys. Lett. B **774**, 103 (2017).

[11] K.-J. Sun, L.-W. Chen, C. M. Ko, J. Pu, and Z. Xu, Light nuclei production as a probe of the QCD phase diagram, Phys. Lett. B **781**, 499 (2018).

[12] H. Liu, D. Zhang, S. He, K.-j. Sun, N. Yu, and X. Luo, Light nuclei production in Au + Au collisions at $\sqrt{s_{\mathrm{NN}}} =$ 5200 GeV from JAM model, Phys. Lett. B **805**, 135452 (2020).

[13] X. Luo, S. Shi, N. Xu, and Y. Zhang, A study of the properties of the QCD Phase diagram in high-energy nuclear collisions, Particles **3**, 278 (2020).

[14] K. Blum, K. C. Y. Ng, R. Sato, and M. Takimoto, Cosmic rays, antihelium, and an old navy spotlight, Phys. Rev. D **96**, 103021 (2017).

[15] V. Poulin, P. Salati, I. Cholis, M. Kamionkowski, and J. Silk, Where do the AMS-02 antihelium events come from?, Phys. Rev. D **99**, 023016 (2019).

[16] V. Vagelli (AMS Collaboration), Results from AMS-02 on the ISS after 6 years in space, Nuovo Cimento C **42**, 173 (2019).

[17] P. J. Siemens and J. I. Kapusta, Evidence for a Soft Nuclear Matter Equation of State, Phys. Rev. Lett. **43**, 1486 (1979).

[18] A. Andronic, P. Braun-Munzinger, J. Stachel, and H. Stocker, Production of light nuclei, hypernuclei and their antiparticles in relativistic nuclear collisions, Phys. Lett. B **697**, 203 (2011).

[19] A. Andronic, P. Braun-Munzinger, K. Redlich, and J. Stachel, The statistical model in Pb-Pb collisions at the LHC, Nucl. Phys. **A904-905**, 535c (2013).

[20] J. Cleymans, S. Kabana, I. Kraus, H. Oeschler, K. Redlich, and N. Sharma, Antimatter production in proton-proton and heavy-ion collisions at ultrarelativistic energies, Phys. Rev. C **84**, 054916 (2011).

[21] P. G. Ortega, D. R. Entem, F. Fernandez, and E. Ruiz Arriola, Counting states and the hadron resonance gas: Does X(3872) count?, Phys. Lett. B **781**, 678 (2018).

[22] P. G. Ortega and E. Ruiz Arriola, Is X(3872) a bound state?, Chin. Phys. C **43**, 124107 (2019).

[23] H. H. Gutbrod, A. Sandoval, P. J. Johansen, A. M. Poskanzer, J. Gosset, W. G. Meyer, G. D. Westfall, and R. Stock, Final State Interactions in the Production of Hydrogen and Helium Isotopes by Relativistic Heavy Ions on Uranium, Phys. Rev. Lett. **37**, 667 (1976).

[24] H. Sato and K. Yazaki, On the coalescence model for high-energy nuclear reactions, Phys. Lett. **98B**, 153 (1981).

[25] S. Mrowczynski, On the neutron proton correlations and deuteron production, Phys. Lett. B **277**, 43 (1992).

[26] L. P. Csernai and J. I. Kapusta, Entropy and cluster production in nuclear collisions, Phys. Rep. **131**, 223 (1986).

[27] S. Mrowczynski, Production of light nuclei in the thermal and coalescence models, Acta Phys. Pol. B **48**, 707 (2017).

[28] S. Bazak and S. Mrowczynski, ^{4}He vs. ^{4}Li and production of light nuclei in relativistic heavy-ion collisions, Mod. Phys. Lett. A **33**, 1850142 (2018).

[29] Z.-J. Dong, G. Chen, Q.-Y. Wang, Z.-L. She, Y.-L. Yan, F.-X. Liu, D.-M. Zhou, and B.-H. Sa, Energy dependence of light (anti)nuclei and (anti)hypertriton production in the Au-Au collision from $\sqrt{s_{NN}} = 11.5$ to 5020 GeV, Eur. Phys. J. A **54**, 144 (2018).

[30] K.-J. Sun and L.-W. Chen, Production of $\Lambda\Lambda$ and $\overline{\Lambda \mathrm{n}}$ in central Pb + Pb collisions at $\sqrt{s_{NN}} = 2.76$ TeV within a covariant coalescence model, Phys. Rev. C **94**, 064908 (2016).

[31] A. Polleri, J. P. Bondorf, and I. N. Mishustin, Effects of collective expansion on light cluster spectra in relativistic heavy ion collisions, Phys. Lett. B **419**, 19 (1998).

[32] S. Mrowczynski and P. Slon, Hadron-deuteron correlations and production of light nuclei in relativistic heavy-ion collisions, Acta Phys. Pol. B **51**, 1739 (2020).

[33] S. Bazak and S. Mrowczynski, Production of ^{4}Li and $p - {}^3$He correlation function in relativistic heavy-ion collisions, Eur. Phys. J. A **56**, 193 (2020).

[34] P. Danielewicz and G. F. Bertsch, Production of deuterons and pions in a transport model of energetic heavy ion reactions, Nucl. Phys. **A533**, 712 (1991).

[35] D. Oliinychenko, L.-G. Pang, H. Elfner, and V. Koch, Microscopic study of deuteron production in PbPb collisions at $\sqrt{s} = 2.76$ TeV via hydrodynamics and a hadronic afterburner, Phys. Rev. C **99**, 044907 (2019).

[36] M. E. Peskin and D. V. Schroeder, *An Introduction to Quantum Field Theory* (Addison-Wesley, Reading, USA, 1995).

[37] U. Wolff, Precision check on triviality of ϕ^4 theory by a new simulation method, Phys. Rev. D **79**, 105002 (2009).

[38] A. Agodi, G. Andronico, P. Cea, M. Consoli, and L. Cosmai, The (lambda Phi**4)(4) theory on the lattice: Effective potential and triviality, Nucl. Phys. B Proc. Suppl. **63**, 637 (1998).

[39] H. Kleinert and V. Schulte-Frohlinde, *Critical Properties of Phi^4-Theories* (World Scientific, 2001), https://doi.org/10.1142/4733.

[40] A. Messiah, *Quantum Mechanics* (Dover Publication, New York, USA, 1999).

[41] F. Giacosa and G. Pagliara, On the spectral functions of scalar mesons, Phys. Rev. C **76**, 065204 (2007).

[42] Y. Burdanov, G. Efimov, S. Nedelko, and S. Solunin, Meson masses within the model of induced nonlocal quark currents, Phys. Rev. D **54**, 4483 (1996).

[43] A. Faessler, T. Gutsche, M. Ivanov, V. E. Lyubovitskij, and P. Wang, Pion and sigma meson properties in a relativistic quark model, Phys. Rev. D **68**, 014011 (2003).

[44] F. Giacosa, T. Gutsche, and A. Faessler, A Covariant constituent quark/gluon model for the glueball-quarkonia content of scalar-isoscalar mesons, Phys. Rev. C **71**, 025202 (2005).

[45] J. R. E. Taylor, *Scattering Theory: The Quantum Theory of Nonrelativistic Collisions* (John Wiley, USA, 1972).

[46] J. B. Hartle and C. E. Jones, Inelastic Levinson's theorem, cdd singularities and multiple resonance poles, Ann. Phys. (N.Y.) **38**, 348 (1966).

[47] M. Wellner, Levinson's Theorem (an elementary derivation), Am. J. Phys. **32**, 787 (1964).

[48] R. Dashen, S.-K. Ma, and H. J. Bernstein, S matrix formulation of statistical mechanics, Phys. Rev. **187**, 345 (1969).

[49] R. Venugopalan and M. Prakash, Thermal properties of interacting hadrons, Nucl. Phys. **A546**, 718 (1992).

[50] W. Broniowski, F. Giacosa, and V. Begun, Cancellation of the σ meson in thermal models, Phys. Rev. C **92**, 034905 (2015).

[51] P. M. Lo, B. Friman, M. Marczenko, K. Redlich, and C. Sasaki, Repulsive interactions and their effects on the thermodynamics of a hadron gas, Phys. Rev. C **96**, 015207 (2017).
[52] P. M. Lo, S-matrix formulation of thermodynamics with N-body scatterings, Eur. Phys. J. C **77**, 533 (2017).
[53] P. M. Lo, B. Friman, K. Redlich, and C. Sasaki, S-matrix analysis of the baryon electric charge correlation, Phys. Lett. B **778**, 454 (2018).
[54] A. Dash, S. Samanta, and B. Mohanty, Interacting hadron resonance gas model in the K -matrix formalism, Phys. Rev. C **97**, 055208 (2018).
[55] A. Dash, S. Samanta, and B. Mohanty, Thermodynamics of a gas of hadrons with attractive and repulsive interactions within an S-matrix formalism, Phys. Rev. C **99**, 044919 (2019).
[56] P. M. Lo and F. Giacosa, Thermal contribution of unstable states, Eur. Phys. J. C **79**, 336 (2019).

Capturing nonexponential dynamics in the presence of two decay channels

Francesco Giacosa [1,2] Przemysław Kościk [3] and Tomasz Sowiński [4]

[1]*Institute of Physics, Jan-Kochanowski University, ulica Uniwersytecka 7, PL-25406 Kielce, Poland*

[2]*Institute for Theoretical Physics, J. W. Goethe University, Max-von-Laue-Strasse 1, DE-60438 Frankfurt am Main, Germany*

[3]*Department of Computer Science, State Higher Vocational School in Tarnów, ulica Mickiewicza 8, PL-33100 Tarnów, Poland*

[4]*Institute of Physics, Polish Academy of Sciences, Aleja Lotników 32/46, PL-02668 Warsaw, Poland*

(Received 13 January 2020; accepted 15 July 2020; published 11 August 2020)

The most unstable quantum states and elementary particles possess more than a single decay channel. At the same time, it is well known that typically the decay law is not simply exponential. Therefore, it is natural to ask how to spot the nonexponential decay when (at least) two decay channels are opened. In this work, we study the tunneling phenomenon of an initially localized particle in two spatially opposite directions through two different barriers, mimicking two decay channels. In this framework, through specific quantum mechanical examples which can be accurately solved, we study the general properties of a two-channel decay that apply for various unstable quantum states (including unstable particles). Apart from small deviations at early times, the survival probability and the partial tunneling probability along the chosen direction are very well described by the exponential-decay model. In contrast, the ratios of the decay probabilities and probability currents are evidently not a simple constant (as they would be in the exponential limit), but display time-persisting oscillations. Hence, these ratios are optimal witnesses of deviations from the exponential-decay law.

DOI: 10.1103/PhysRevA.102.022204

I. INTRODUCTION

The fact that the decay law in quantum mechanics (QM) is not described by an exponential function is well established [1–13]. In particular, decaying systems very often exhibit the *Zeno period* at short initial times, in which the nondecay probability, i.e., the probability $p(t)$ that the unstable particle prepared at the initial time $t = 0$ has not decayed yet at a later time $t > 0$, is quadratic in time, $p(t) - 1 \propto -t^2$. On the other hand, for very long times (typically several orders of magnitude larger than the lifetime [2]), the nondecay probability is typically governed by a power law. From the experimental point of view, the deviations from the exponential decay have been verified at short times in the study of tunneling of sodium atoms in an optical potential [14] and, more recently, in the study of decays of unstable molecules via the emission of photons [15]. Even if ubiquitous from a theoretical point of view, in physical systems the deviations from the exponential case are typically very small, making them very difficult to be measured.

Quite remarkably, the nonexponential decay also allows one to influence the decay rate by changing the way the measurement is performed. As examples, the famous Quantum Zeno Effect (QZE) and the Inverse Zeno Effect (IZE) are direct consequences of the peculiarity of the decay law [16–27] . Indeed, experimental confirmation of both the QZE and the IZE was achieved in experiments in which electrons undergo a Rabi transition between atomic energy levels [28–30]. In these cases, the nondecay probability oscillates in time as $\sim\cos^2(\Omega t)$ and is evidently nonexponential. Even if this is not a real unstable system, the slowdown of the quantum transition by frequent measurements could be seen in these experiments. Even more interestingly, these effects were also confirmed in the tunneling of sodium atoms, which represent a genuine irreversible quantum decay [31]. Finally, the QZE and IZE are also related to the quantum computation and quantum control, which are important elements in this flourishing research field [32,33].

Deviations from the exponential-decay law are indeed expected also in quantum field theory (QFT), which is the ultimate correct framework to study the creation and annihilation of particles, and hence the decay of unstable particles [10,34,35]. Namely, even if a perturbative treatment is not capable to capture such deviations [36], the spectral function in QFT is not a Breit-Wigner [37–39] and, in some cases, it can be very different from it [40]. As a consequence, the decay law is also not a simple exponential. Unfortunately, a direct experimental proof of the nonexponential decay of unstable elementary particles is still missing. Nonetheless, the Zeno effect confirmed recently in cavity QED [41] suggests that different dynamical features of the simplest QM systems may also have their counterparts in different purely QFT situations.

An interesting case is realized when an unstable quantum state (or particle) can decay in (at least) two channels. Indeed, this situation takes place very often in Nature. For instance, in the realm of particle physics, most unstable particles possess multiple decay channels [42]. Similarly, electrons in excited atoms can decay in more than a single energy level [43].

As expected, in the exponential limit, the ratio of the decay probabilities into the first and the second channel is a constant. A detailed study of the nonexponential decay when two (or more) decay channels are present is described in [10]. In QM, this ratio is not a constant, but shows some peculiar and irregular oscillations, which in [10] were discussed in the framework of the so-called Lee model [44,45] (also called the Friedrichs model or the Jaynes-Cummings model [43,46]),

which captures the most salient features of QFT (for details, see [10,47–50]). Moreover, qualitatively similar results for the ratio of the partial decay probability currents were obtained in [10], also in a quantum field theoretical model. Yet, the topic of nonexponential decay in the presence of more decay channels needs novel and different studies that will allow us to understand, in more detail, its features and make an experimental verification (or falsification) possible.

In this work, we explore the two-channel decay problem in a quantum mechanical context. To this aim, we introduce a simple model of a single particle initially confined in a box potential whose walls are suddenly partially released, allowing the particle to tunnel to the open space. In this way, we slightly generalize the celebrated *Winter's model* [3], where only a single box wall is released. The Winter model is recognized as one of the most important workhorses in the theory of nonexponential decays (see, for example, [4–9] and [51] for a general treatment). In our work, we want to mimic two different channels of a decay and therefore we focus on situations of essentially different barriers. In contrast to the symmetric situation of identical barriers [52–54], in this case the exact analytical solution is known only for the scattering problem of external wave packets [55–59] and it does not provide a straightforward solution for the decay scenario studied here [60]. Specifically, using (in numerical means) the corresponding time-dependent Schrödinger equation, we check how to capture deviations from the exponential-decay law. In agreement with Ref. [10], but with a different method, we find that the ratio of the decay probability currents shows time-persisting deviations from the exponential-decay law predictions. The main advantage of the approach presented here is its complete transparency of all successive steps and its feasibility in physical experiments in which the tunneling in different directions can be obtained by asymmetric potentials. Moreover, as discussed in the summary, the qualitative features of the obtained results are expected to be quite general and can be used not only to describe the generic tunneling processes of particles to the open space, but also to understand decays of unstable relativistic particles in the QFT language.

II. THE MODEL

In this paper, we consider a single particle moving in a one-dimensional space subjected to two separated δ potential barriers. The system is described by the following Hamiltonian:

$$\mathcal{H} = -\frac{\hbar^2}{2m}\frac{d^2}{dx^2} + V_L\delta(x+R) + V_R\delta(x-R), \tag{1}$$

where R is the half distance between the two barriers and their height is controlled by the independent parameters V_L and V_R. Our aim is to find the decay properties of a particle that is initially located between the barriers. To this aim, at the initial moment ($t = 0$), the wave function is taken as

$$\Psi(x, t=0) = \Psi_0(x) = \begin{cases} \frac{1}{\sqrt{R}}\cos\left(\frac{\pi x}{2R}\right), & |x| \leqslant R \\ 0, & |x| > R, \end{cases} \tag{2}$$

which corresponds to the ground state in the limit of barriers of infinite heights. This choice is quite natural, but of course one could use other initial wave functions without changing the qualitative results that we are going to present.

The properties of the studied system are controlled by only two independent dimensionless parameters. It is clearly visible that all quantities can be expressed in units fixed by the half distance R. Namely, if all distances are measured in units of R, energies in units of $\hbar^2/(mR^2)$, and time intervals in units of $mR^2/\hbar$, then the properly rescaled (dimensionless) Hamiltonian takes the form

$$\mathcal{H} = -\frac{1}{2}\frac{d^2}{dx^2} + V_0[\delta(x+1) + \kappa\delta(x-1)], \tag{3}$$

where $V_0 = \frac{mR}{\hbar^2}V_L$ and $\kappa = V_R/V_L$ are two independent dimensionless parameters controlling the heights of the left barrier and the ratio between the right and the left heights, respectively. In these units, we solve the time-dependent Schrödinger equation,

$$(i\partial_t - \mathcal{H})\Psi(x,t) = 0, \tag{4}$$

with the initial wave function (2). Notice that in the chosen units, the initial energy of the system (in the limit $V_0 \to \infty$, and $\kappa > 0$) is $E_0 = \pi^2/8$, which is of the order of 1. Clearly, due to the mirror symmetry of the problem, without losing generality, one can restrict to $0 < \kappa \leqslant 1$.

To quantify the dynamics of the system, we focus our attention on *the nondecay probability* defined as

$$P_0(t) = \int_{-1}^{+1} dx\,|\Psi(x,t)|^2, \tag{5}$$

i.e., the probability that the particle is remaining in the region $x \in (-1, 1)$ at the time t. Note that this quantity is interchangeably also called *the survival probability*, but then some attention is needed [61]. Moreover, we also consider the left and the right decay probabilities defined as

$$P_L(t) = \int_{-\infty}^{-1} dx\,|\Psi(x,t)|^2, \tag{6a}$$

$$P_R(t) = \int_{+1}^{+\infty} dx\,|\Psi(x,t)|^2, \tag{6b}$$

where $P_L(t)$ ($P_R(t)$) is the probability that at the time t, the particle can be found to the left (right) of the well, i.e., it is the probability that the tunneling to the left (right) has occurred in the time interval between 0 and t. Obviously, at any instant t, these probabilities are not independent and must obey the normalization condition

$$P_0(t) + P_L(t) + P_R(t) = 1. \tag{7}$$

It is also extremely useful to consider the probability currents (the time derivatives of the probabilities) describing the speed of their temporal change,

$$p_0(t) = -\frac{dP_0(t)}{dt}, \quad p_L(t) = \frac{dP_L(t)}{dt}, \quad p_R(t) = \frac{dP_R(t)}{dt}. \tag{8}$$

Notice that the definition of $p_0(t)$ takes into account that the nondecay probability decreases with time. Temporal changes of $p_0(t)$ are often measured in experiments since it corresponds to the number of decay products per unit of time (for instance, the lifetime measurement of the neutron by the beam

method [62] or the decay of H-like ions via electron capture and neutrino emission [63]). Note that a simple interpretation holds: $p_{L(R)}(t)dt$ is the probability that the decay occurs to the right (left) between t and $t+dt$. Clearly, from the relation (7), one finds that

$$p_0(t) = p_L(t) + p_R(t). \tag{9}$$

The central quantities that we focus on in the following are the right-to-left ratio of probabilities,

$$\mathbf{\Pi}(t) = \frac{P_R(t)}{P_L(t)}, \tag{10}$$

and its counterpart, the right-to-left ratio of probability currents,

$$\boldsymbol{\pi}(t) = \frac{p_R(t)}{p_L(t)}. \tag{11}$$

It will turn out that the time dependence of both ratios plays a crucial role in capturing the nonexponential-decay behavior of the system.

Finally, let us recall the explicit forms of all these functions when the exponential Breit-Wigner (BW) limit [64–66] holds. In this limit, the nondecay probability reads

$$P_0(t) \xrightarrow{\text{BW}} e^{-\Gamma t}, \tag{12}$$

where Γ is the decay rate. As argued in [2], the exponential dependence of the nondecay probability is a direct consequence of the Breit-Wigner energy distribution of the unstable state. The decay rate Γ can also be decomposed to partial decay rates to the "left" Γ_L and to the "right" Γ_R associated with these two distinguished decay channels, $\Gamma = \Gamma_L + \Gamma_R$. Then, the partial decay probabilities have the form

$$P_L(t) \xrightarrow{\text{BW}} \frac{\Gamma_L}{\Gamma}(1 - e^{-\Gamma t}), \tag{13a}$$

$$P_R(t) \xrightarrow{\text{BW}} \frac{\Gamma_R}{\Gamma}(1 - e^{-\Gamma t}). \tag{13b}$$

Obviously, the partial decay probability currents read

$$p_L(t) \xrightarrow{\text{BW}} \Gamma_L e^{-\Gamma t}, \quad p_R(t) \xrightarrow{\text{BW}} \Gamma_R e^{-\Gamma t}. \tag{14}$$

For future convenience, we introduce the ratio of the partial decay widths,

$$\beta = \Gamma_R/\Gamma_L, \tag{15}$$

which, in the BW limit, remains constant and directly connects the right-to-left ratios (10) and (11),

$$\mathbf{\Pi}(t) = \frac{P_R(t)}{P_L(t)} \xrightarrow{\text{BW}} \beta \xleftarrow{\text{BW}} \frac{p_R(t)}{p_L(t)} = \boldsymbol{\pi}(t). \tag{16}$$

To show that the exponential-decay law is violated, it is sufficient to expose deviations from the constant value of $\beta = \Gamma_R/\Gamma_L$. This is why the right-to-left ratios (10) and (11) are of special interest.

III. RESULTS

We solve the Schrödinger equation (4) by expressing the time-dependent wave function in terms of eigenstates of the dimensionless Hamiltonian (3). In practice, due to a lack of convenient exact analytical solutions, we diagonalize it on a finite spatial interval with closed boundaries at $x = \pm L$ with $L/R \gg 1$ (for more technical details, see the Appendix). We then calculate the nondecay probability $P_0(t)$, the partial decay probabilities $P_L(t)$ and $P_R(t)$, and, finally, the two ratios $\mathbf{\Pi}(t)$ and $\boldsymbol{\pi}(t)$.

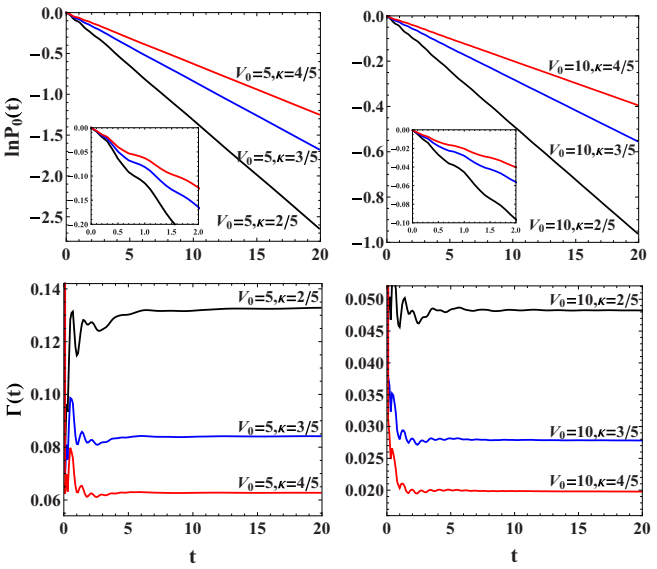

FIG. 1. Upper panels: The nondecay probability $P_0(t)$ as a function of time for some chosen values of κ and V_0. The insets highlight the behavior at short times. Bottom panels: The corresponding results for the decay rate $\Gamma(t) = -\ln P_0(t)/t$.

In the upper panel of Fig. 1, we show the nondecay probability $P_0(t)$ as a function of time for some chosen values of V_0 and κ (the insets highlight the changes for small t). It is clearly seen that after a short initial period, $P_0(t)$ exhibits an exponential decay. It is even more evident when the decay rate $\Gamma(t) = -\ln P_0(t)/t$ is plotted (bottom panel in Fig. 1)—after some small initial wiggles, it reaches a constant value, indicating a quite fast transition to the BW regime. These results suggest that in the regime of exponential decay, the approximation (12) should be applied. It turns out that in this regime, the nondecay probability almost ideally fits the relation

$$P_0(t) \approx e^{-\Gamma(t-t_0)}, \tag{17}$$

manifesting the correctness of the BW limit predictions. Note that in general the additional "time shift" t_0 is nonzero and its inverse is directly related to the initial period of nonexponential decay. In fact, the sign of t_0 indicates if, for small times, the dynamics is sub- or supexponential (see [22] and [46] for detailed discussions of this point). In the cases studied here, this parameter is very close to 0 and, due to numerical uncertainty, we are not able to determine its sign. To gain a deeper insight into the validity of the BW approximation, we additionally check how the ratio of partial decay rates β depends on κ and V_0 (see Fig. 2). It turns out that the ratio β becomes insensitive to changes in V_0 when V_0 is large enough. In fact, for a considered range of κ, the changes in V_0 do not affect the value of β when V_0 exceeds a value

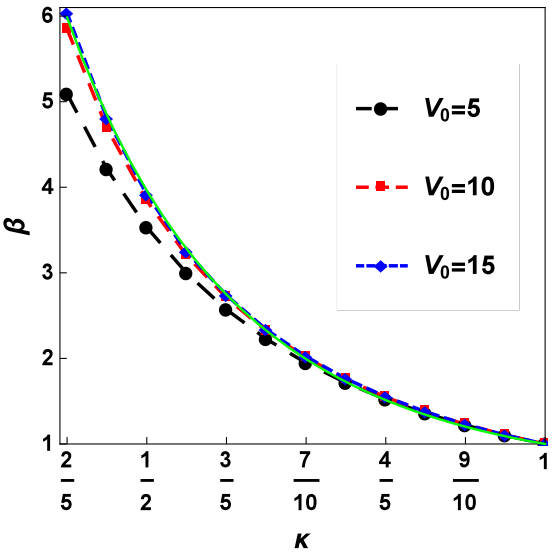

FIG. 2. The ratio of partial decay rates β calculated in the BW limit as a function of the asymmetry parameter κ for different values of V_0. The green solid line indicates a phenomenological relation $\beta = \kappa^{-2}$ justified in the limit of large V_0.

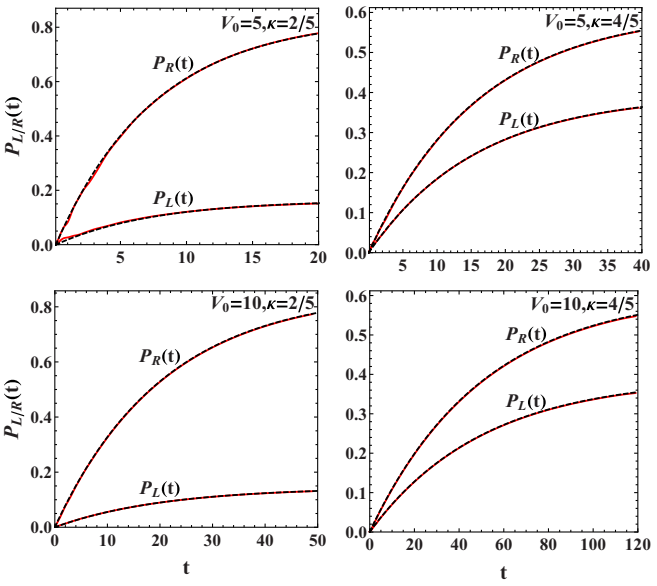

FIG. 3. Partial decay probabilities $P_R(t)$ and $P_L(t)$ as a function of time. Note that accurate numerical results (continuous black lines) coincidence with predictions of the BW limit (13) (red dashed lines). See the main text for details.

of about 15. Moreover, in this regime, the ratio β, when treated as a function of κ, almost perfectly follow the simple relation $\beta(\kappa) \approx \kappa^{-2}$ (green line in Fig. 2). This relation has a direct intuitive phenomenological explanation. For large V_0, tunnelings in opposite directions become almost independent and therefore the ratio of tunneling amplitudes is simply given by the ratio of the barrier heights, κ^{-1}. It means that the ratio of probabilities is controlled solely by κ^{-2}.

The discussion above means that the exponential formula provides a very good approximation for large enough (but not too large) times. Clear deviations are visible only for initial moments (for the cases studied, $t \lesssim 5$). Of course, the deviations become larger for smaller V_0. However, we focus on the cases in which $P_0(t)$ is almost exponential since this is the typically realized scenario in Nature.

The situation is very similar when partial decay probabilities (6) are considered. In this case, after fitting to appropriate exponential functions of the form

$$P_{L/R}(t) \approx \frac{\Gamma_{L/R}}{\Gamma}[1 - e^{-\Gamma(t-t_0)}], \tag{18}$$

we see full agreement of the BW limit predictions with accurate numerical results (see Fig. 3 for comparison).

All three results presented for probabilities $P_0(t)$, $P_R(t)$, and $P_L(t)$ suggest that any discrepancies from the exponential behavior are poorly captured by these quantities. We checked that this is also the case when the probability currents (8), i.e., the temporal derivatives of the probabilities, are considered. However, the situation changes dramatically when, instead of pure probabilities (probability currents), the properties of their temporal ratios $\mathbf{\Pi}(t)$ and $\boldsymbol{\pi}(t)$ are investigated. In Fig. 4, we present accurate numerical results for these ratios as a function of time for the same set of parameters as in Fig. 1. One can see that the ratios $\mathbf{\Pi}(t)$ and $\boldsymbol{\pi}(t)$ have rather complex behavior, especially for the initial period. More importantly, the deviations from the constant value obtained in the exponential BW limit are clearly visible. Both functions eventually reach the expected constant value of β in the limit of large times. Note, however, that here we do not consider very large times in which the decay is again nonexponential due to the onset of a power law. In our studies, when referring to intermediate and large times, we mean periods in which the decay is almost ideally exponential.

In fact, our results allow us to conclude that partial probabilities $P_L(t)$ and $P_R(t)$ are generally linearly independent functions since, if $\mathbf{\Pi}(t)$ and $\boldsymbol{\pi}(t)$ are not identically equal, then the Wronskian $W(t) = P_L(t)p_R(t) - P_R(t)p_L(t)$ is not singular. [Note that for $\kappa = 1$, symmetric tunneling to the left and to the right occurs: $\mathbf{\Pi}(t) = \boldsymbol{\pi}(t) = 1$]. Only for a very large time, when both ratios reach an almost constant value β, one finds that $\mathbf{\Pi}(t) - \boldsymbol{\pi}(t) \approx 0$, which means that

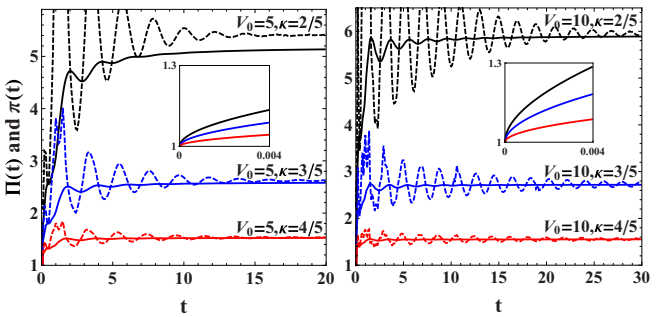

FIG. 4. Temporal ratio of partial probabilities $\mathbf{\Pi}(t)$ (continuous lines) and partial probability currents $\boldsymbol{\pi}(t)$ (dashed lines) as functions of time for the same set of parameters as in Fig. 1. The insets highlight the short-time behavior. Both quantities oscillate at intermediate times but the ratio $\boldsymbol{\pi}(t)$ shows evident deviations from the BW limit predictions even for very long times.

partial probabilities $P_R(t)$ and $P_L(t)$ behave as nearly linear-dependent functions.

In particular, the right-to-left probability currents ratio $\boldsymbol{\pi}(t)$ shows evident oscillations persisting for a very long time. It means that it is an appropriate quantity to exhibit deviations from the exponential BW limit predictions, even in moments when the standard nondecay probability $P_0(t)$, the partial decay probabilities $P_R(t)$ and $P_L(t)$, or even their ratio $\boldsymbol{\Pi}(t)$ are not able to capture this behavior. Let us also recall that the ratio $\boldsymbol{\pi}(t)$ has a straightforward physical meaning. For the time intervals in which $\boldsymbol{\pi}(t) > \beta$ [$\boldsymbol{\pi}(t) < \beta$], the particle decay to the right is more [less] probable than naively expected from the exponential law. Then, the value of β has only an appropriate interpretation as an average ratio. Closer inspection of Fig. 4 shows additional interesting insights for the function $\boldsymbol{\pi}(t)$. Namely, the amplitude of oscillations does not decrease in the limit of large V_0 as long as κ is sufficiently different from unity. Namely, when it approaches 1, the ratio $\boldsymbol{\pi}(t)$ rapidly flattens around the expected value 1. Consequently, in these cases, the deviations from the expected constant limit become very small.

The above analysis shows that the ratios $\boldsymbol{\Pi}(t)$ and $\boldsymbol{\pi}(t)$ can be regarded as appropriate quantities capturing nonexponential decay in the presence of two decay channels. However, as we argued, the ratio of the time derivatives $\boldsymbol{\pi}(t)$ is much more sensitive to nonexponential features of the system than the direct ratio of probabilities $\boldsymbol{\Pi}(t)$. Therefore, from the experimental point of view, if one aims to validate exponential decay, the largest effort should be put toward accurate determination of the quantity $\boldsymbol{\pi}(t)$ rather than $\boldsymbol{\Pi}(t)$.

It is interesting to note that for a given asymmetry of the barriers κ, the amplitude of the oscillations is not strongly dependent on V_0. For example, as presented in Fig. 4, the amplitudes for $V_0 = 5$ and $V_0 = 10$ are not much different when the same value of $\kappa = 2/5$. In contrast, the frequency of the oscillations is essentially affected by the choice of V_0 and it is larger for stronger V_0. The latter observation implies that for very large V_0, experimental detection of oscillations will be very challenging due to the finite resolution of time probes. Simply, to have any realistic chance to detect the effect, a period of the oscillation should not be smaller than the experimental time resolution.

Importantly, it should be pointed out here that in our work, we do not consider deviations from the exponential decay occurring always for very large times, i.e., when the decay is characterized by the power law rather than the exponential one [1,3,15]. In fact, this regime is not well captured in our analysis due to the numerical simplification of the model described in the Appendix. Although going beyond this approximation is straightforward, it highly increases the numerical complexity without changing the results in the time ranges that we are interested in. Therefore, the discussion of properties of the ratios $\boldsymbol{\Pi}(t)$ and $\boldsymbol{\pi}(t)$ for very long times is beyond the scope of this work.

One can expect that the qualitative features of the results obtained do not significantly depend on the details of the employed decay model. This conviction is justified since the origin of the different behavior of $\boldsymbol{\pi}(t)$ and $\boldsymbol{\Pi}(t)$ is ingrained in the fundamental properties of the two-channel decay, rather than a particular physical realization. Note that both quantities are described by the same decay width β only in the BW limit independently in the underlying model. It means that any deviation from this prediction is a direct manifestation of the nonexponential decay. In other words, as long as the probabilities for the two partial decay channels are not equal, the corresponding functions $P_L(t)$ and $P_R(t)$ approach the respective exponential limits in a slightly different way. Consequently, ratios $\boldsymbol{\Pi}(t)$ and $\boldsymbol{\pi}(t)$ are characterized by slightly different and time-dependent parameters. This is the intuitive reason why the ratios enhance the differences quite independently of the details of a model. This is also one of the reasons why very similar results were obtained in a completely different context in [10] in the framework of the Lee model [44] containing essential simplification when compared to the generalized Winter's model considered here. In contrast to the case studied, in the Lee model it is assumed that there exists the unique *unstable* state $|\psi_0\rangle$ decaying to two different subspaces (channels L and R) spanned by states $|k, L\rangle$ and $|k, R\rangle$ having the same dispersion relation $\omega(k)$. In such a case, the Hamiltonian of the system can be written explicitly in the basis of these states as

$$\mathcal{H}_{\text{Lee}} = E_0|\psi_0\rangle\langle\psi_0| + \sum_{\sigma\in\{L,R\}}\int_0^\infty dk\,\omega(k)|k,\sigma\rangle\langle k,\sigma| + \sum_{\sigma\in\{L,R\}}\int_0^\infty dk\,[f_\sigma(k)|k,\sigma\rangle\langle\psi_0| + f_\sigma^*(k)|\psi_0\rangle\langle k,\sigma|], \tag{19}$$

where $f_\sigma(k) = \langle k,\sigma|H|\psi_0\rangle$ are transition amplitudes controlling tunneling through the barriers. The nonexponential decay observed in these two, essentially different models suggests once more that our findings on properties of ratios $\boldsymbol{\pi}(t)$ and $\boldsymbol{\Pi}(t)$ persist model independently.

IV. CONCLUSIONS

In this work, we analyzed the general problem of capturing nonexponential properties in the presence of the two-channel decay process. Taking as a working horse a very simple dynamical problem of a single particle flowing out from a leaky box, we examined direct relations between the probabilities of tunneling to the right and the left as functions of the control parameters. In this way, we studied relations between partial decays into two distinct channels in a relatively simple system, which allows for a very accurate numerical treatment. Since the multiple channel decay of an unstable quantum state is a very frequent problem in QM and QFT, the results can be important for our understanding of a broad range of physical phenomena.

The results obtained confirm that in the presence of two decay channels, the system exhibits a remarkable nonexponential behavior on long timescales. Even in cases where the simplest quantities do not reveal any nonexponential signatures, the interchannel ratio of probability currents $\boldsymbol{\pi}(t)$ directly exposes these features. Importantly, this quantity, although not the simplest property of the system, is almost directly measurable in experiments [67–69]. Therefore, it can

be viewed as a possible *smoking gun* of nonexponential-decay behavior.

It is worthwhile to point out that the model discussed in this work, although seemingly oversimplified, to some extent can be realized experimentally and gives prospects for direct verification of our predictions. State-of-the-art experiments [70–73] with ultracold atoms confined in optical traps allow one to prepare quasi-one-dimensional uniform box traps where particles are confined. Moreover, the outside walls of these traps can be controlled independently and released almost on-demand, opening direct routes to realize our model. Another interesting direction of experimental realization is to analyze different nuclei with nonsymmetric few-channel decays, for instance, the decay of α particle in large nonspherical nuclei.

From a theoretical point of view, one can easily extend the present work to more complicated (and more realistic) forms of asymmetric potentials. While any qualitative differences from the results obtained are not expected, such studies would help to establish a closer relevance to upcoming experimental schemes. From the conceptual side, extensions of the results to higher dimensions are also straightforward. Another promising route for further explorations is to study analogous systems containing several interacting particles [74–85] and pin down the role of the quantum statistics. Furthermore, the topic should also be reinvestigated in the realm of QFT to shed some fresh light on the problem of multichannel decays of elementary particles and composite hadrons.

ACKNOWLEDGMENTS

F.G. thanks G. Pagliara, M. Piotrowska, and K. Kulińska-Maciejska for useful discussions. T.S. acknowledges financial support from the (Polish) National Science Center under Grant No. 2016/22/E/ST2/00555.

APPENDIX: NUMERICAL APPROACH

Numerical calculations are performed in the basis of the eigenstates of the Hamiltonian (3) diagonalized numerically on a finite spatial interval with closed boundary conditions at $x = \pm L$. Everywhere besides the points $x = \pm 1$, the Hamiltonian is equivalent to the Hamiltonian of a free particle. Therefore, any of its eigenstates can be expressed as follows:

$$\psi(x) = \begin{cases} A\sin[p(L+x)] & \text{if } x < -1 \\ B\sin[p(L-x)] & \text{if } x > 1 \\ C\sin(px) + D\cos(px) & \text{if } |x| \leqslant 1, \end{cases} \tag{A1}$$

where parameters A, B, C, and D are established in such a way that the wave function fulfills continuity conditions at positions of the left and the right barrier. These four conditions read

$$\lim_{\epsilon\to 0}[\psi(-1+\epsilon) - \psi(-1-\epsilon)] = 0, \tag{A2a}$$

$$\lim_{\epsilon\to 0}\left[\frac{d}{dx}\psi(x)\Big|_{-1+\epsilon} - \frac{d}{dx}\psi(x)\Big|_{-1-\epsilon}\right] = 2V_L\psi(-1), \tag{A2b}$$

$$\lim_{\epsilon\to 0}[\psi(1+\epsilon) - \psi(1-\epsilon)] = 0, \tag{A2c}$$

$$\lim_{\epsilon\to 0}\left[\frac{d}{dx}\psi(x)\Big|_{1+\epsilon} - \frac{d}{dx}\psi(x)\Big|_{1-\epsilon}\right] = 2V_R\psi(1), \tag{A2d}$$

and they lead to the homogenous system of linear equations of the form $\mathcal{M}\cdot\vec{v} = 0$, where $\vec{v} = (A, B, C, D)^T$ and

$$\mathcal{M} = \begin{pmatrix} \frac{1}{2}p\cos[(L-1)p] & 0 & -\frac{1}{2}p\cos(p) - V_L\sin(p) & V_L\cos(p) - \frac{1}{2}p\sin(p) \\ 0 & -\frac{1}{2}p\cos[(L-1)p] & \frac{1}{2}p\cos(p) + V_R\sin(p) & V_R\cos(p) - \frac{1}{2}p\sin(p) \\ \sin[(L-1)p] & 0 & \sin(p) & -\cos(p) \\ 0 & -\sin[(L-1)p] & -\sin(p) & -\cos(p) \end{pmatrix}.$$

In this way, the allowed momenta p_i and the corresponding coefficients $\vec{v}_i$ are determined. Then, the the time-dependent wave function is simply given as

$$\Psi(x,t) = \sum_i \alpha_i \exp\left(-it\,p_i^2/2\right)\psi_i(x), \tag{A3}$$

where the expansion coefficients α_i are determined by the initial wave function (2). The accuracy of the final results is easily controlled (and, if needed, may be straightforwardly improved) by changing the number of terms in the expansion (A3). Typically, in our calculations, we use 3000 terms and $L = 400$–600, which is sufficient to achieve well-converged results avoiding reflections at the walls at $x = \pm L$ for large t. The method used assures a full control on the accuracy of the final results.

[1] L. A. Khalfin Decay theory of a quasi-stationary state, Zh. Eksp. Teor. Fiz. **33**, 1371 (1957) [Sov. Phys. JETP **6**, 1053 (1958)].

[2] L. Fonda, G. C. Ghirardi, and A. Rimini, Decay theory of unstable quantum systems, Rep. Prog. Phys. **41**, 587 (1978).

[3] R. G. Winter, Evolution of a Quasi-Stationary State, Phys. Rev. **123**, 1503 (1961).

[4] J. Levitan, Small time behavior of an unstable quantum system, Phys. Lett. A **129**, 267 (1988).

[5] D. A. Dicus, W. W. Repko, R. F. Schwitters, and T. M. Tinsley, Time development of a quasi-stationary state, Phys. Rev. A **65**, 032116 (2002).

[6] M. Peshkin, A. Volya, and V. Zelevinsky, Nonexponential and oscillatory decays in quantum mechanics, Europhys. Lett. **107**, 40001 (2014).

[7] A. Wyrzykowski, Analysis of the breakdown of exponential decays of resonances, arXiv:1801.02350.

[8] G. García-Calderón, and R. Romo, Nonexponential tunneling decay of a single ultracold atom, Phys. Rev. A **93**, 022118 (2016).

[9] T. Koide and F. M. Toyama, Decay process accelerated by tunneling in its very early stage, Phys. Rev. A **66**, 064102 (2002).

[10] F. Giacosa, Nonexponential decay in quantum field theory and in quantum mechanics: The case of two (or more) decay channels, Found. Phys. **42**, 1262 (2012).

[11] F. Giacosa, Energy uncertainty of the final state of a decay process, Phys. Rev. A **88**, 052131 (2013).

[12] K. Raczynska and K. Urbanowski, Survival amplitude, instantaneous energy and decay rate of an unstable system: Analytical results, Acta Phys. Polon. B **49**, 1683 (2018).

[13] F. V. Pepe, P. Facchi, Z. Kordi, and S. Pascazio, Nonexponential decay of Feshbach molecules, Phys. Rev. A **101**, 013632 (2020).

[14] S. R. Wilkinson, C. F. Bharucha, M. C. Fischer, K. W. Madison, P. R. Morrow, Q. Niu, B. Sundaram, and M. G. Raizen, Experimental evidence for non-exponential decay in quantum tunnelling, Nature (London) **387**, 575 (1997).

[15] C. Rothe, S. I. Hintschich, and A. P. Monkman, Violation of the Exponential-Decay Law at Long Times, Phys. Rev. Lett. **96**, 163601 (2006).

[16] A. Degasperis, L. Fonda, and G. C. Ghirardi, Does the lifetime of an unstable system depend on the measuring apparatus? Nuovo Cim. A **21**, 471 (1973).

[17] B. Misra and E. C. G. Sudarshan, The zeno's paradox in quantum theory, J. Math. Phys. **18**, 756 (1977).

[18] A. Kofman and G. Kurizki, Acceleration of quantum decay processes by frequent observations, Nature (London) **405**, 546 (2000).

[19] A. Kofman and G. Kurizki, Acceleration of quantum decay processes by frequent observations, Z. Naturforsch. A **56** (2001).

[20] K. Koshino and A. Shimizu, Quantum Zeno effect by general measurements, Phys. Rep. **412**, 191 (2005).

[21] D. Solokovski, M. Pons, and T. Kamalov, Anomalous Zeno effect for sharply localised atomic states, arXiv:1203.5632.

[22] P. Facchi and S. Pascazio, Quantum Zeno dynamics: Mathematical and physical aspects, J. Phys. A **41**, 493001 (2008).

[23] P. Facchi and S. Pascazio, Acceleration of quantum decay processes by frequent observations, Fortschr. Phys. **49**, 941 (2001).

[24] P. Facchi, H. Nakazato, and S. Pascazio, From the Quantum Zeno to the Inverse Quantum Zeno Effect, Phys. Rev. Lett. **86**, 2699 (2001).

[25] L. S. Schulman, Continuous and pulsed observations in the quantum Zeno effect, Phys. Rev. A **57**, 1509 (1998).

[26] F. Giacosa and G. Pagliara, Pulsed and continuous measurements of exponentially decaying systems, Phys. Rev. A **90**, 052107 (2014).

[27] F. Giacosa and G. Pagliara, Neutron decay anomaly and inverse quantum Zeno effect, Phys. Rev. D **101**, 056003 (2020).

[28] W. M. Itano, D. J. Heinzen, J. J. Bollinger, and D. J. Wineland, Quantum Zeno effect, Phys. Rev. A **41**, 2295 (1990).

[29] C. Balzer *et al.*, The quantum Zeno effect - Evolution of an atom impeded by measurement, Optics Commun. **211**, 235 (2002).

[30] E. W. Streed, J. Mun, M. Boyd, G. K. Campbell, P. Medley, W. Ketterle, and D. E. Pritchard, Continuous and Pulsed Quantum Zeno Effect, Phys. Rev. Lett. **97**, 260402 (2006).

[31] M. C. Fischer, B. Gutierrez-Medina, and M. G. Raizen, Observation of the Quantum Zeno and Anti-Zeno Effects in an Unstable System, Phys. Rev. Lett. **87**, 040402 (2001).

[32] G. A. Paz-Silva, A. T. Rezakhani, J. M. Dominy, and D. A. Lidar, Zeno Effect for Quantum Computation and Control, Phys. Rev. Lett. **108**, 080501 (2012).

[33] P. Facchi, G. Marmo, and S. Pascazio, Quantum Zeno dynamics and quantum Zeno subspaces, J. Phys.: Conf. Ser. **196**, 012017 (2009).

[34] P. Facchi and S. Pascazio, Van Hove's "$\lambda 2t$" limit in nonrelativistic and relativistic field theoretical models, Chaos Solitons Fractals **12**, 2777 (2001).

[35] F. Giacosa and G. Pagliara, Deviation from the exponential decay law in relativistic quantum field theory: the example of strongly decaying particles, Mod. Phys. Lett. A **26**, 2247 (2011).

[36] C. Bernardini, L. Maiani, and M. Testa, Short time behavior of unstable systems in field theory and proton decay, Phys. Rev. Lett. **71**, 2687 (1993).

[37] P. T. Matthews and A. Salam, Relativistic field theory of unstable particles, Phys. Rev. **112**, 283 (1958).

[38] P. T. Matthews and A. Salam, Relativistic theory of unstable particles., Phys. Rev. **115**, 1079 (1959).

[39] F. Giacosa and G. Pagliara, On the spectral functions of scalar mesons, Phys. Rev. C **76**, 065204 (2007).

[40] J. R. Pelaez, From controversy to precision on the sigma meson: A review on the status of the nonordinary $f_0(500)$*resonance*, Phys. Rep. **658**, 1 (2016).

[41] J. Bernu, S. Deléglise, C. Sayrin, S. Kuhr, I. Dotsenko, M. Brune, J. M. Raimond, and S. Haroche, Freezing Coherent Field Growth in a Cavity by the Quantum Zeno Effect, Phys. Rev. Lett. **101**, 180402 (2008).

[42] M. Tanabashi *et al.*, The review of particle physics, Phys. Rev. D **98**, 030001 (2018).

[43] M. Scully and M. Zubairy, *Quantum Optics* (Cambridge University Press, Cambridge, 1997).

[44] T. D. Lee, Some special examples in renormalizable field theory, Phys. Rev. **95**, 1329 (1954).

[45] C. B. Chiu, E. C. G. Sudarshan, and G. Bhamathi, The Cascade model: A Solvable field theory, Phys. Rev. D **46**, 3508 (1992).

[46] A. G. Kofman, G. Kurizki, and B. Sherman, Spontaneous and induced atomic decay in photonic band structures, J. Mod. Opt. **41**, 353 (1994).

[47] Z. W. Liu, W. Kamleh, D. B. Leinweber, F. M. Stokes, A. W. Thomas, and J. J. Wu, Hamiltonian Effective Field Theory Study of the N(1535) Resonance in Lattice QCD, Phys. Rev. Lett. **116**, 082004 (2016).

[48] Z. Xiao and Z. Y. Zhou, On Friedrichs model with two continuum states, J. Math. Phys. **58**, 062110 (2017).

[49] Z. Y. Zhou and Z. Xiao, Understanding X(3862), X(3872), and X(3930) in a Friedrichs-model-like scheme, Phys. Rev. D **96**, 054031 (2017).

[50] P. M. Lo and F. Giacosa, Thermal contribution of unstable states, Eur. Phys. J. C **79**, 336 (2019).

[51] M. Razavy, *Quantum Theory of Tunneling* (World Scientific, Singapore, 2003).

[52] D. Bauch, The path integral for a particle moving in a δ-function potential, Nuov. Cim. B **85**, 118 (1985).

[53] Yu. N. Demkov and V. N. Ostrovskii, *Zero-Range Potentials and Their Applications in Atomic Physics* (Springer, Boston, 1988).

[54] M. Kleber, Exact solutions for time-dependent phenomena in quantum mechanics, Phys. Rep. **236**, 331 (1994).

[55] J. Mateos Guilarte and J. M. Muñoz-Castañeda, Double-delta potentials: One-dimensional scattering, Int. J. Theor. Phys. **50**, 2227 (2011).

[56] Z. Ahmed, S. Kumar, M. Sharma, and V. Sharma, Revisiting double Dirac delta potential, Eur. J. Phys. **37**, 045406 (2006).

[57] Y. Nogami and C. K. Ross, Scattering from a nonsymmetric potential in one dimension as a coupled-channel problem, Am. J. Phys. **64**, 923 (1996).

[58] I. Yanetka, On the transmission coefficient for the double delta-function potential, Acta Phys. Pol. A **97**, 1053 (2000).

[59] F. Erman, M. Gadella, S. Tunali, and H. Uncu, A singular one-dimensional bound state problem and its degeneracy, Eur. Phys. J. Plus **132**, 352 (2017).

[60] The problem of adaptation of the general scattering solutions reported in, e.g., Ref. [55] to the problem of decay studied here originates in the lack of orthogonality between left-to-right and right-to-left scattering solutions. Finding an orthogonal and complete basis is not an easy task since the orthogonalizing transformation is momentum dependent. More precisely, the problem can be, as expected, solved in the symmetric case: The sum and the difference of the scattering wave solutions are even and odd functions, respectively, and hence they are orthogonal and the desired basis can be found. However, in the general (and, for us, crucial) asymmetric case, this is not possible: For each momentum k, a different field transformation should be performed and it is at present unclear how to handle the problem. (Note that the standard Gram-Schmidt method does not apply for states whose norm is infinite.) In view of these difficulties, since the numerical solutions that we provide are correct and since the derivation of the analytic solution is, albeit interesting and desirable, not central for our goals, we decided to leave this task for the future.

[61] There is a subtle but important difference between the nondecay and the survival probability at a given time t. The former is the probability that no decay has occurred at t, and the latter that the particle occupies the same initial state. In this sense, Eq. (5) defines the nondecay probability, while the survival probability is defined as $P_{\rm surv}(t) = |\int_{-1}^{+1} dx \Psi_0(x)\Psi(x,t)|^2$. Clearly, for the system studied, the nondecay probability is the natural quantity to consider.

[62] A. T. Yue, M. S. Dewey, D. M. Gilliam, G. L. Greene, A. B. Laptev, J. S. Nico, W. M. Snow, and F. E. Wietfeldt, Improved Determination of the Neutron Lifetime, Phys. Rev. Lett. **111**, 222501 (2013).

[63] F. C. Ozturk *et al.*, New test of modulated electron capture decay of hydrogen-like ^{142}Pm ions: Precision measurement of purely exponential decay, Phys. Lett. B **797**, 134800 (2019).

[64] V. Weisskopf and E. P. Wigner, Calculation of the natural brightness of spectral lines on the basis of Dirac's theory, Z. Phys. **63**, 54 (1930).

[65] V. Weisskopf and E. Wigner, Over the natural line width in the radiation of the harmonius oscillator, Z. Phys. **65**, 18 (1930).

[66] G. Breit, Theory of resonance reactions and allied topics, Handbuch Phys. **41**, 1 (1959).

[67] S. Murmann, A. Bergschneider, V. M. Klinkhamer, G. Zürn, T. Lompe, and S. Jochim, Two Fermions in a Double Well: Exploring a Fundamental Building Block of the Hubbard Model, Phys. Rev. Lett. **114**, 080402 (2015).

[68] L. Fallani, C. Fort, J. Lye, and M. Inguscio, Bose-Einstein condensate in an optical lattice with tunable spacing: Transport and static properties, Opt. Express **13**, 4303 (2005).

[69] I. Kuzmenko, T. Kuzmenko, Y. Avishai, and Y. B. Band, Atoms trapped by a spin-dependent optical lattice potential: Realization of a ground-state quantum rotor, Phys. Rev. A **100**, 033415 (2019).

[70] J. J. P. van Es, P. Wicke, A. H. van Amerongen, C. Rétif, S. Whitlock, and N. J. van Druten, Box traps on an atom chip for one-dimensional quantum gases, J. Phys. B: At., Mol. Opt. Phys. **43**, 155002 (2010).

[71] A. L. Gaunt, T. F. Schmidutz, I. Gotlibovych, R. P. Smith, and Z. Hadzibabic, Bose-Einstein Condensation of Atoms in a Uniform Potential, Phys. Rev. Lett. **110**, 200406 (2013).

[72] L. Chomaz, L. Corman, T. Bienaimé, R. Desbuquois, C. Weitenberg, S. Nascimbéne, J. Beugnon, and J. Dalibard, Emergence of coherence via transverse condensation in a uniform quasi-two-dimensional Bose gas, Nat. Commun. **6**, 6162 (2015).

[73] B. Mukherjee, Z. Yan, P. B. Patel, Z. Hadzibabic, T. Yefsah, J. Struck, and M. W. Zwierlein, Homogeneous Atomic Fermi Gases, Phys. Rev. Lett. **118**, 123401 (2017).

[74] P. Kościk and A. Okopińska, Two-electron entanglement in elliptically deformed quantum dots, Phys. Lett. A **374**, 3841 (2010).

[75] A. del Campo, F. Delgado, G. Garcia-Calderon, J. G. Muga, and M. G. Raizen, Decay by tunneling of bosonic and fermionic Tonks-Girardeau gases, Phys. Rev. A **74**, 013605 (2006).

[76] A. U. J. Lode, A. I. Streltsov, O. E. Alon, H.-D. Meyer, and L. S. Cederbaumet, Exact decay and tunneling dynamics of interacting few-boson systems, J. Phys. B **42**, 044018 (2009).

[77] S. Kim and J. Brand, Decay modes of two repulsively interacting bosons, J. Phys. B **19**, 195301 (2011)

[78] T. Maruyama, T. Oishi, K. Hagino, and H. Sagawa, Time-dependent approach to many-particle tunneling in one dimension, Phys. Rev. C **86**, 044301 (2012).

[79] A. U. J. Lode, S. Klaiman, O. E. Alon, A. I. Streltsov, and L. S. Cederbaum, Controlling the velocities and the number of emitted particles in the tunneling to open space dynamics, Phys. Rev. A **89**, 053620 (2014).

[80] S. E. Gharashi and D. Blume, Tunneling dynamics of two interacting one-dimensional particles, Phys. Rev. A **92**, 033629 (2015).

[81] R. Lundmark, C. Forssen, and J. Rotureau, Tunneling theory for tunable open quantum systems of ultracold atoms in one-dimensional traps, Phys. Rev. A **91**, 041601(R) (2015).

[82] A. U. J. Lode, *Tunneling Dynamics in Open Ultracold Bosonic Systems* (Springer International, New York, 2015).

[83] I. S. Ishmukhamedov and V. S. Melezhik, Tunneling of two bosonic atoms from a one-dimensional anharmonic trap, Phys. Rev. A **95**, 062701 (2017).

[84] J. Dobrzyniecki and T. Sowiński, Dynamics of a few interacting bosons escaping from an open well, Phys. Rev. A **98**, 013634 (2018).

[85] J. Dobrzyniecki and T. Sowiński, Momentum correlations of a few ultra-cold bosons escaping from an open well, Phys. Rev. A **99**, 063608 (2019).